CFD and FEM Analysis of Passive Variable Flow Controller

Yucan Ding[1], Victor Petrov[1], and Brendan Kochunas[1]

[1]*University of Michigan*

09/15/2023

This page is intentionally blank.

REVISION LOG

Revision	Date	Affected Pages	Revision Description
0	09/15/2023	All	Initial Release

Document pages that are:

|	
Export Controlled:	None
IP/Proprietary/NDA Controlled:	None
Sensitive Controlled:	None
Unlimited:	All

EXECUTIVE SUMMARY

In this report we develop a novel design for a passively controlled valve that utilizes different shapes of the bimetallic vane-based controller inside the cooling channel. By taking advantage of the deformation characteristic of the bimetallic vane, additional flow areas would be generated to allow more coolant to flow. The pressure drop across the cooling channel would also decrease accordingly, which allows more heat transfer to take place, and eventually, realize the purpose of reactivity control.

The basic concept of the passive variable flow controller valve is illustrated in Fig. EC.1.

The summary of the contributions of this report are:

- Identification of materials suitable for bimetallic valve devices

- Optimization of a passive flow controller design for reactivity control

- Detailed sensitivity analysis of parameters affecting controller performance

The work documented here is primarily contained in two other publications included as appendices. The first appendix is a master's thesis report from University of Michigan that was the main mechanism for conducting this work. The second appendix is a corresponding NURETH article based on this work.
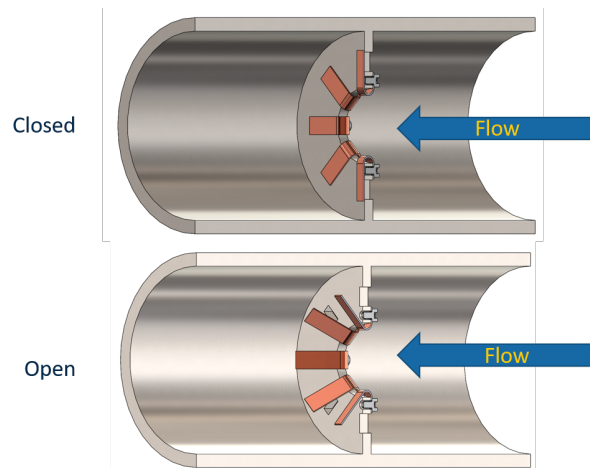
Figure EC.1. Illustration of Principal Mechanics of Bi-metallic Flow Controller

The report (with appendices) describes Finite Element Method (FEM) simulations to evaluate the deflection of bimetallic membranes for multiple materials, shapes, and thicknesses Further, Computational Fluid Dynamics (CFD) simulations for various flow controller shapes and configurations to work towards optimization of the device geometry from a flow control capabilities standpoint are documented. The flow control capabilities were evaluated based on the pressure drop across the fully open and fully closed device for different fluid mass flow rates and temperatures. Preliminary results show a good device candidate that allows to reach up to three times in pressure drop difference between fully closed and fully open devices.

The feasibility of the device was tested using CFD and FEM simulations, demonstrating that such a straightforward device geometry could provide a pressure drop alteration of up to 46%-56%, depending on the selected geometry and temperature over a broad range of flow velocities. It is critical to note that the proposed geometries are conceptual studies and not the final designs, and careful consideration should be given to material selection to ensure good corrosion and fatigue resistance in the flow media and certain operating conditions. Therefore, measures would also be needed to prevent electrochemical corrosion at the bonding layer of the bimetallic strip or at the interface, for example, using thin buffer layers or encapsulating strips. Lastly, any radiation enhanced fatigue or corrosion effects would need to be studied and measured carefully.

A possible direction for future work regarding the utilization of bimetallic devices for flow control could involve investigating various engineering approaches to use bimetallic features as motion actuators. These actuators could be mounted outside of the actual flow and actuated thermally through heat conduction through the walls. This approach might help reduce the requirement for high corrosion resistance if the valve is in the flow; however, additional attention would need to be given to sealing the moving parts.

This page is intentionally blank.

COLLEGE OF ENGINEERING
NUCLEAR ENGINEERING & RADIOLOGICAL SCIENCES
UNIVERSITY OF MICHIGAN

CONTENTS

ACRONYMS

FEM Finite Element Method

CFD Computational Fluid Dynamics

NEUP Nuclear Energy University Partnership

MPC Model Predictive Control

1. INTRODUCTION

The overall objective of this Nuclear Energy University Partnership (NEUP) is conduct research into solutions for semi-autonomous or autonomous microreactors. Broadly, in this project we have understood a key challenge in such a capability to be to perform load-follow maneuvers without human intervention. To that end, we have considered multiple approaches. One approach documented in several other project reports [1, 2] and papers [3, 4] used state-of-the-art Model Predictive Control (MPC) algorithms to determine what systems to actuate in the reactor.

This report focuses on a complementary or alternative approach based on a passive reactivity control system. The basic principal of this system is to use bimetallic vanes to change the pressure drop, and thus mass flow rate in the primary loop based on the reactor inlet temperature.

In performing the feasibility studies documented in this report, we considered the target reactor to be the Holos-quad reactor developed by HolosGen, LLC. An illustration of this reactor is shown in Fig. 1 and a system diagram with nominal operating conditions is shown in Fig. 2.
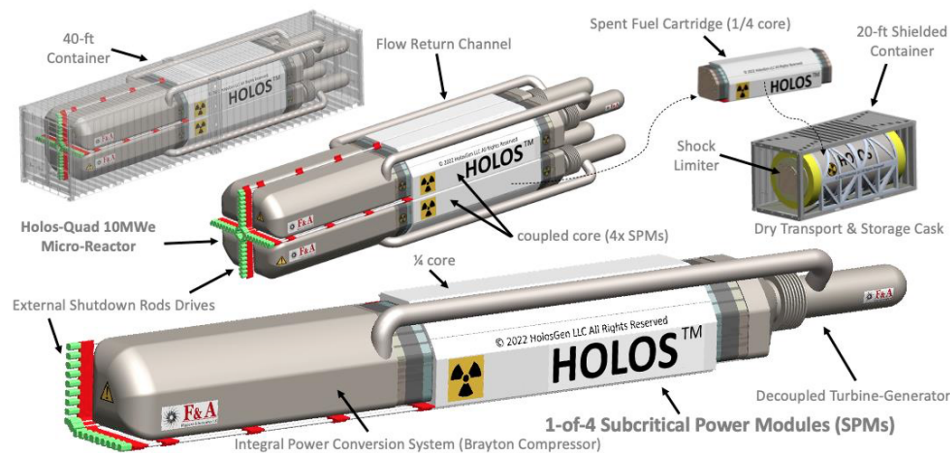
Figure 1. Overview of Holos-Quad (Gen 2+) subcritical power modules [5, 6]
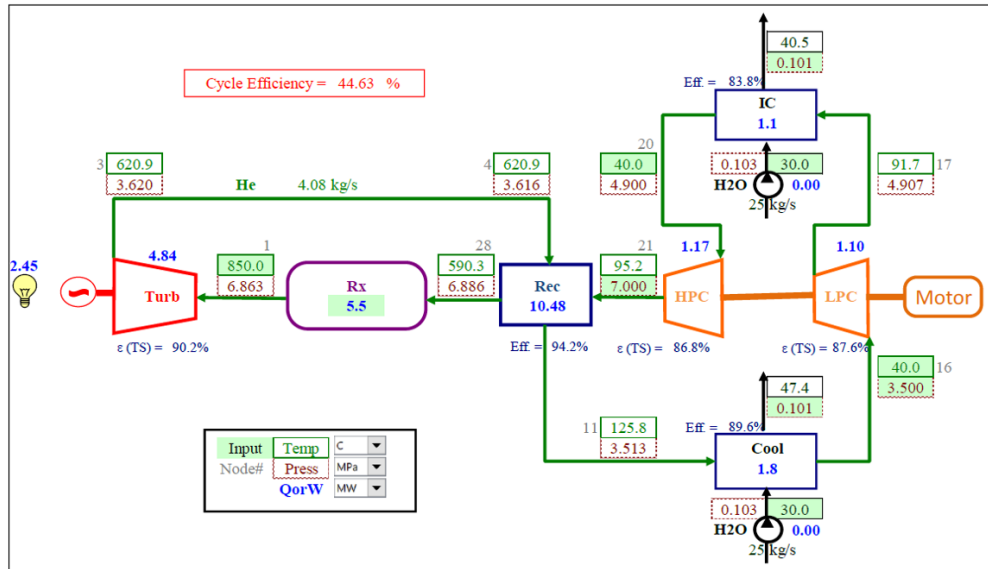
Figure 2. Holos-Quad SPM system design and Design Conditions [7]

Much of the work relevant to this milestone task has been previously documented in two publications. The first is a master's thesis from the University of Michigan. The second is an extended summary recently presented at the 20th International Topical Meeting on Nuclear Reactor Thermal Hydraulics (NURETH-20). Therefore, we refer the reader to these two appendices for the detailed description of the work performed to complete this milestone.

ACKNOWLEDGEMENTS

Nuclear Reactor
Analysis & Methods
Group NuRAM

COLLEGE OF ENGINEERING
NUCLEAR ENGINEERING & RADIOLOGICAL SCIENCES
UNIVERSITY OF MICHIGAN

REFERENCES

[1] S. Choi, S. Kinast, and K. B. "Point Kinetics Model Development with Predictive Control for Multi-Module HTGR Special Purpose Reactors." Technical Report NURAM-2020-006-00, University of Michigan (2020).

[2] S. Choi, Q. Shen, L. C.H., and B. Kochunas. "High Fidelity Transient Simulations of the Multi-module HTGR Special Purpose Reactor." Technical Report NURAM-2023-006-00, University of Michigan (2023).

[3] S. Choi, S. Kinast, C. Filippone, , and B. Kochunas. "Comparative Study for Load-follow Operations of the Holos Microreactor." In *Proc. M&C 2021* (2021).

[4] S. Choi, Q. Shen, C.-H. Lee, C. Filippone, , and B. Kochunas. "Preliminary Results of Load Follow Simulation for Holos-Quad Microreactor using PROTEUS and Model Predictive Control." In *Proc. M&C 2023* (2023).

[5] N. Stauff, C. Lee, and C. Filippone. "Core Design of the Holos-Quad Microreactor." Technical Report ANL/NSE-22/4, Argonne National Lab.(ANL), Argonne, IL (United States) (2022).

[6] "HolosGen LLC." URL http://www.holosgen.com.

[7] A. Moisseytsev and C. Filippone. "Load Following Analysis of the Holos-Quad 10MWe Micro-Reactor with Plant Dynamics Code." Technical Report ANL/NSE-21/32, Argonne National Lab.(ANL), Argonne, IL (United States) (2022).

APPENDIX A

NERS 799 Final Report Study of a Novel Variable Flow Controller-Based Passive Control System Using Bimetallic Vanes

NERS 799

Study of a Novel Variable Flow Controller-Based Passive Control System Using Bimetallic Vanes

Final Report

UM ID: 42261411

Name: Yucan Ding

Unique Name: ycding@umich.edu

Instructor: Dr. Victor Petrov & Dr. Annalisa Manera

Contents

1. Introduction

1.1 Background

A fine-controlled reactivity level in the nuclear reactor has always been one of the most significant practices under different working conditions. To achieve this goal, a novel design of the passively controlled system that applies different shapes of the bimetallic-vane-based controller inside the cooling channel has been proposed. By taking advantage of the deformation characteristic of the bimetallic vane, additional flow areas would be generated to allow more coolant to flow. The pressure drop across the cooling channel would also decrease accordingly, which allows more heat transfer to take place, and eventually, realize the purpose of reactivity control.

Although there have been related studies to investigate variable heat transfer features within the reactor's cooling channels by applying passively controlled systems, specific research for using bimetallic valves in the high-pressure and high-radioactive reactor atmospheres is relatively limited. Among those previous studies, Pattison et al. (2015) used bimetallic strips as thermally actuated valves in an auto thermal microchannel reactor [1], proving that the thermally actuated valves can adequately control reactor temperatures during disturbances in flow rate to the reforming channel. Pattison et al.'s study mainly focused on microchannel reactors, especially the chemical processing part within it, which has unique geometry and industrial application compared with other types of nuclear reactors. Nevertheless, this study proved the applicability of using passively controlled valves within the channel to adjust the heat transfer within the channels. Verstraete et al. (2013) studied maximizing the heat transfer performance by performing multi-objective optimization of a U-bend in internal cooling channels [2], the enhancement of this design ranged from roughly 12~30% decrease in total pressure loss and an 8~17% increase in heat flow rate, while the drawback was that a fixed geometry cannot enable optimal operation under different working conditions.

1.2 Objective

This study aims at studying and testing various novel bimetallic-vane-based passive control systems within the cooling channel. By simulating the internal flow process, properties, especially the pressure drop along the cooling channel, were monitored under

different inlet velocities to evaluate the performance of each passive control system. To conduct the simulations, numbers of FEM models with different thicknesses and material types were created first to conduct the thermal analysis, then the corresponding deformation models were imported to commercial Computational Fluid Dynamics (CFD) code STAR-CCM+ to run the CFD simulations. This paper will first introduce how were the FEM and CFD models established in Sections 2 and 3, including material selection and mesh generation, then compare the pressure drop data among different controller designs to prove the system's applicability in Section 4.

2. FEM Modeling

2.1 Geometry and Experimental Setup

Typically, bimetallic strips use two types of materials with significant thermal expansion coefficient variance, which enables the bimetallic strip to convert the temperature change into the deformation of the structure. In the originally designed system, 8 U-shape "flower-vane-shape" bimetal vanes are mounted in a non-inclined controller within the coolant channel (Fig. 1). The shorter end of the vane (see Fig. 2) is mounted on the controller, while the longer end is not fixed. Different shapes of the controllers will be introduced and tested in the following sections. Assuming that the vanes are not deformed at the initial temperature, as the temperature increases, the vanes will deform in a certain direction. In this study, we set the thermal expansion coefficient of the outer part's material always less than that of the inner part's material. Therefore, heating the valve results in the U-shape vanes becoming V-shape, which opens extra flow windows in the channel consequently. The additional flow area would reduce the pressure drop across the cooling channel and enhance heat transfer accordingly.
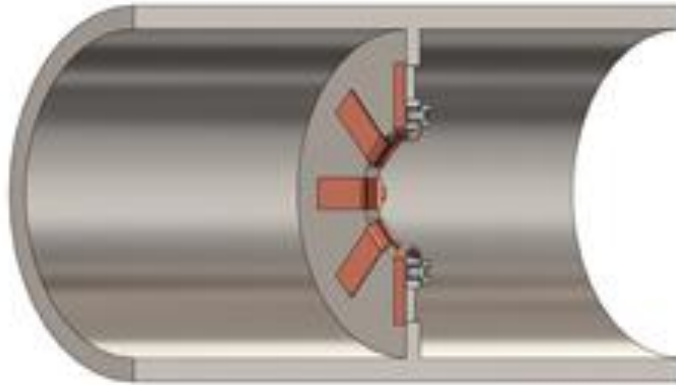
Fig. 1: Sketch of the Bimetal Valve (half) in the Cooling Channel

As shown in Fig. 1, one passively controller in the channel has eight vanes that are mounted on it, these vanes are the same in materials type, geometry, and initial temperature, etc. To simplify the simulation, it is reasonable to study one vane's deformation after heating instead of the whole controller. Before deformation, the geometry size of the 3-D valve model is approximately 25mm×16mm×4mm (see Fig. 2.), while the thickness is subject to change, the initial thickness is 2.5mm. Finite Element Method (FEM) models are established based on the given geometry in ANSYS Workbench to test the maximum deflection that can be reached after temperature increases, then the deformation models will be imported to STAR-CCM+ for further CFD analysis.
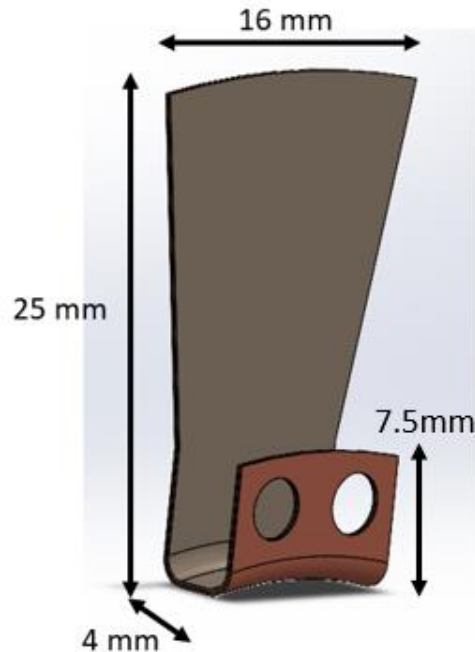

Fig. 2: Sketch of Non-deformed Valve

To test the pressure drop and mass flow rate when fixing this controller (see Fig. 1) within the cooling channel, also considering the symmetric characteristic of the structure, we use a quarter cylinder as the channel and set the controller at the center of the channel (Fig. 3). Two quarter-circle surfaces are set as the inlet and the outlet of the flow. As the temperature increases, water can not only flow through the center quarter circle but also through the extra window that appeared as a result of the vanes deformation. The deformation level of the vanes is obtained from the simulation results in the following sections.
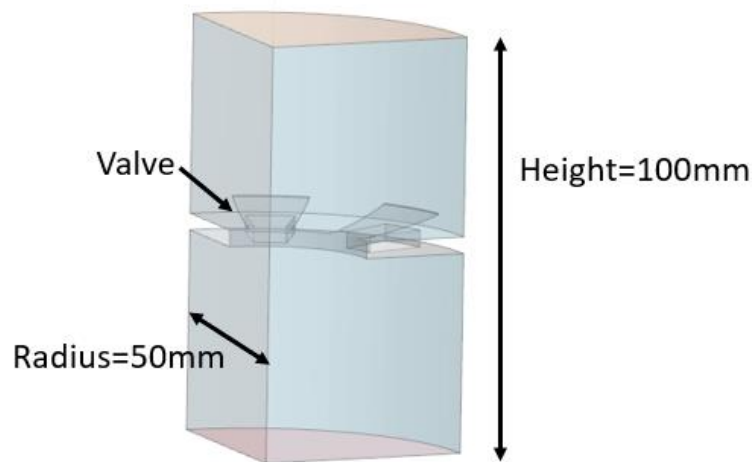

Fig. 3: Flow Channel with Valve

2.2 Material Selection

The choice of the bimetal valve's material plays a critical role in the study. Different aspects should be taken into consideration, including thermal properties, bending ability, and applicability in nuclear reactors, etc.

2.2.1 Thermal Properties

To achieve a reasonable flow area under certain temperature difference, it is necessary to select two materials which

- has a significant difference in physical properties such as thermal expansion coefficient, and Young's modulus, etc.;
- can never completely overlap at any of the temperatures in the operating range;

- is easy to manufacture and at a low cost.

In the previous studies, numerous materials were tested by the researchers to find suitable materials with the characteristics mentioned above. At an early stage, Kumar et al. (2021) [14] carried out a comparative analysis of deflection in bimetals using different material pairs. They tested the Stainless Steel-Copper pair and Stainless Steel-Aluminum pair using commercial finite element modeling software ANSYS and proved that the variation in deflection is mainly due to differences in thermal conductivity, coefficient of thermal expansion, density, and specific heat, etc., the simulation results fitted the theory well. Arnaud et al. (2015) [11] tried different materials to increase the thermo-mechanical efficiencies of the bimetallic strip heat engines, they found that Invar (FeNi36) was an ideal material to be used; Hsu et al. (2002) [12] studied how membrane thickness would influence the performance of the Fe-Ni-Cr/Invar bimetal freestanding membrane, they proved that Invar as one material of the bimetallic tool can always have reliable performance in different conditions; Panowicz et al. (2016) [13] performed the numerical analysis of temperature influence on deformation of the bimetallic element, they tested Invar – Incoloy pair, the results showed that this pair performs well in a wide temperature range.

In sum, among all possible options, Invar has great physical and chemical properties, especially its low thermal expansion coefficient ($1.2 \times 10^{-6} K^{-1}$, around 10 times less than the ordinary steel). It has been widely used in many industrial fields, including chemistry, electricity, and energy. In this study, Invar was set as one of the materials in the bimetal valve.

2.2.2 Applicability in Nuclear Reactor

The high pressure and high irradiation reactor environment make certain types of materials get thermal fatigue, irradiation damage, or creep easily. Thus, these specific materials should be removed from the selection list of the valve's material. For example, some alloys may not be ideal materials due to the high level of absorption of neutrons.

Generally, materials used in nuclear reactors should simultaneously withstand the effects of gamma radiation, high temperature, high pressure, etc., and more importantly, capture very few neutrons to maintain the chain reactions. The major requirements for the in-core material are concluded as:

- Low absorption of neutrons;
- Low corrosion with coolant, fuel, etc.;

5

- Stability under neutron and gamma irradiation;

- Good anti-creep and anti-fatigue characteristic

Van Der Schaaf et al. (1988) [15] tested the effect of neutron irradiation on the fatigue and fatigue-creep behavior of structural materials of the reactor, they tried the following materials: austenitic stainless steel, ferritic martensitic steel, low activation steel, and vanadium base alloys, etc. They proved that austenitic stainless steel could produce inter-granular creep cracks, which formation will be enhanced by radiation-induced segregation on grain boundaries; while low activation steel and vanadium base alloys creep-fatigue interaction is expected to be less severe because of the retarded creep crack development, and ferritic stainless steel is also expected that neutron irradiation will have a limited effect on creep-fatigue interaction. Thus, these certain types of stainless steel are among the ideal options for the material.

The ideal material, e.g., Invar, ferritic stainless steel, is expected to satisfy the above requirements.

2.3 Mesh Sensitivity Test (FEM Model)

The FEM models generated by SolidWorks previously were imported to ANSYS Workbench to generate the mesh and run thermal analysis. The global size ranges from 0.10 mm to 1.00 mm were used to evaluate the maximum deflection, strain, and stress value, respectively. The proper values were chosen based on the tendency of the curves. In this test, the initial temperature was 50℃ and the external temperature load was 280℃; the thickness of the model was 0.3 mm; Invar and ferritic stainless steel were used as the bimetal vane's material. The test results are shown in Fig. 4.
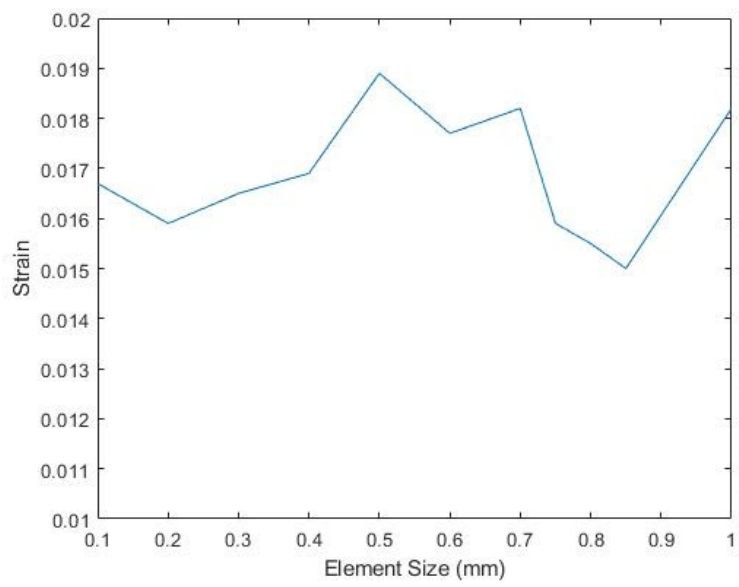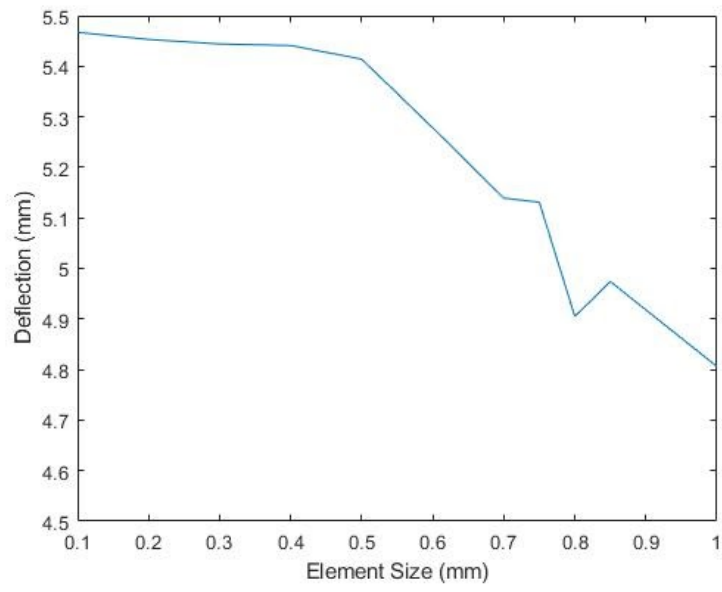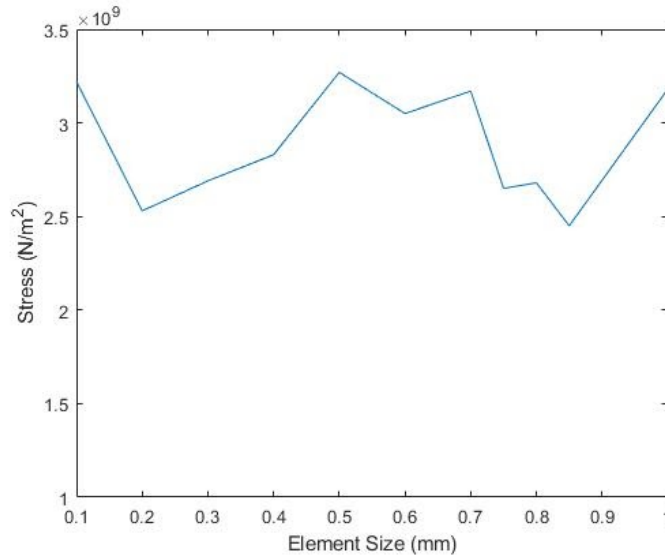
Fig. 4: Mesh Sensitivity Study in FEM Model

As shown in Fig. 4, it is clear that when reducing the element size below and equal to 0.4 mm, the maximum deformation and strain value doesn't change significantly, while there is no clear trend for the variance of stress under different element sizes. Thus, we can conclude that it is a convergence, and continuing to reduce the element size will have little influence on these three criteria and will only increase the computation cost. On the other hand, the values are not stable for all three curves for element sizes larger than 0.40 mm, either. Thus, it is reasonable to set the element size of the FEM model as 0.40 mm. The corresponding maximum deflection value will be used to create the deformation models for further CFD analysis. The original FEM mesh model with 0.4 mm base size generated by ANSYS Workbench is shown in Fig. 5.
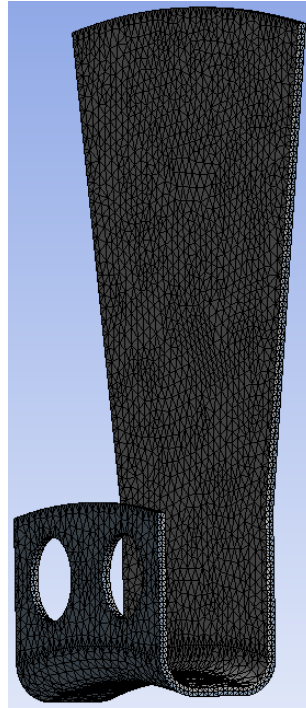
Fig. 5: Mesh Scene of FEM Model

Some of the prospective material pairs were tested in ANSYS Workbench. The working condition including initial temperature, external temperature load, and thickness of the model was all the same as mentioned above. The materials which were used for the outer part of the bimetal vane were all set as Invar. The obtained maximum displacement results are listed in Table 1.

Table 1: Maximum Displacement of Bimetal Valves with Different Materials

Inner Side Material	Inner Material Thermal Expansion Coefficient (1/K)	Maximum Displacement (mm)
Copper	2.4×10^{-5}	10.320
Titanium Ti-8Al-1Mo-1V	8.0×10^{-6}	2.992
Ductile Iron	1.1×10^{-5}	4.144
Stainless Steel (ferritic)	1.1×10^{-5}	5.441

From the obtained data, the Copper – Invar material pair has the largest maximum displacement among all options. Nevertheless, considering that copper is easy to

corrosion by water, it is not an ideal material within the coolant channel. For other pairs, considering ferritic stainless steel has more extraordinary thermal fatigue resistance, etc., characteristic than ductile iron, therefore, we select Invar and stainless steel as the materials of the bimetallic valve in the following study. This deformation model was created and imported to conduct further CFD simulation.

3. CFD Modeling

3.1 Physical Model

The physical model should be selected based on the Reynolds number. In this study, the Reynolds number is at least 50,000 (for the smallest test inlet velocity), which is larger than the common turbulence criteria, Re = 2300. Among all different turbulence models, the k-ω model predicts well near the wall, while it is not an ideal selection far from the wall. In contrast, the standard k-ε model predicts well far from the wall, while it is not sensitive to the rotation and swirl of the flow due to the isotropic nature of its turbulent viscosity, it needs wall treatment to compensate for the inaccuracy near the wall. Therefore, to achieve a better performance, the realizable k-ε model, combined with the two-layer all y+ wall treatment was selected. The previous study [10] has proved that this turbulence model performs well, especially in simulating the velocity field and pressure field of channels with vanes.

A summary of all physical models used in STAR-CCM+ is shown in the table below.

Table 2: Physical Models Implementation

Two-Layer All y+ Wall Treatment	Wall Distance
Realizable k-epsilon Two Layer	K-Epsilon Turbulence
Reynolds-Averaged Navier-Stokes	Turbulent
Constant Density	Gradients
Segregated Flow	Liquid
Steady	Solution Interpolation
Three Dimensional	

3.2 Boundary Conditions

Dozens of surfaces are created in the geometry in STAR-CCM+, each boundary has an imposed boundary condition. Among these surfaces, most of them are simply wall conditions, except an inlet velocity condition range from 0.5 m/s to 1.5 m/s which is imposed for the inlet of the coolant, and the pressure boundary condition imposed for the outlet of the coolant.

3.3 CFD Mesh Model

To obtain an accurate CFD simulation result, the design and refinement of the computational mesh are of great importance. An ideal option of the mesh is considering the computational cost, convergence for the results, etc., at the same time. Thus, a balance of the mesh density and computation cost needs to be reached.

The computational mesh for this study mainly includes the following parts: the ordinary region, the refinement region which is near the vanes, and the prism layer mesh. The base size of the refinement region is manually set as 25% of the base size of the ordinary mesh. By applying this guidance, a sketch of the mesh and the refinement region model generated in STAR CCM+ is shown in the figures below.
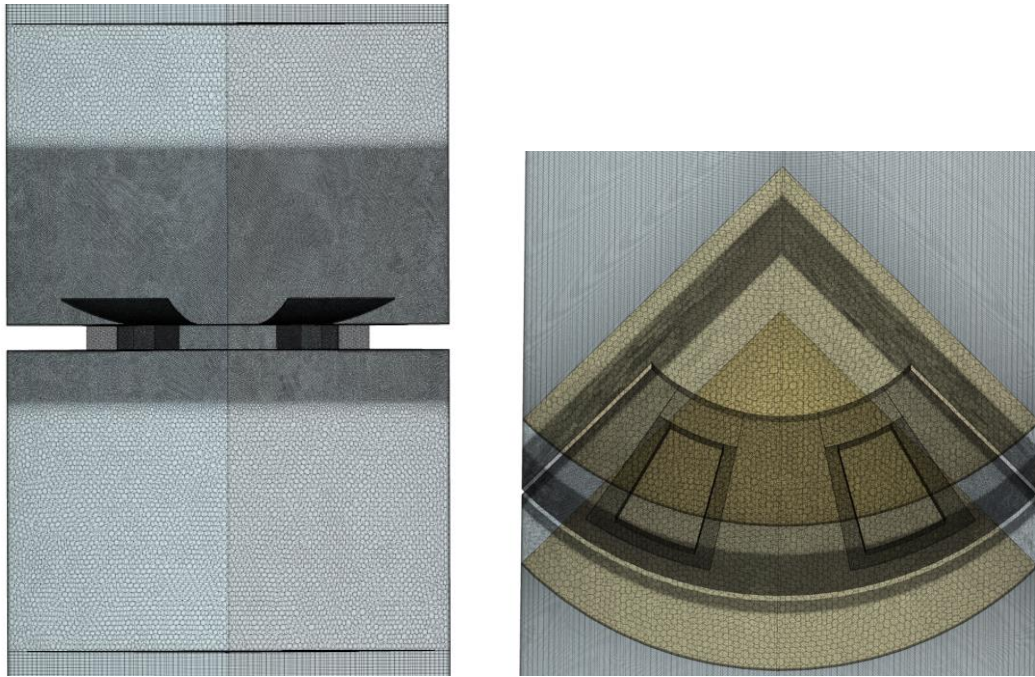

Fig. 6: Sketch of Mesh Sense of CFD Model

3.4 CFD Mesh Sensitivity Test

The general steps for the mesh sensitivity study are: create a coarse mesh first, fix the number of the prism layer, and change the base size to find the optimal value, then fix the base size to find the optimal number of prism layer. In this study, the inlet velocity of 1.5 m/s is selected to do the convergence test.

First, the value of base size is studied, the number of prism layers is initially set as 5. The base tested in this study ranges from 0.8 mm to 1.6 mm. The effect of the computational cost is also considered, and the table that the number of cells changes with the mesh's base size is shown below. When base size reduces 50% percent, the number of cells becomes over 5 times larger than the original one.

Table 3: Number of Cells vs. Base Size

Base Size (mm)	Cell
0.8	8957951
1.0	5267787
1.2	3425307
1.4	2399981
1.6	1761200

To find out the suitable base size, the number of prism layers is set as 5. As shown in Fig. 6, the pressure drop variance is relatively large when the base size is within 1.2 mm to 1.6 mm. However, continuing to reduce the base size when the base size is less than or equal to 1.0 mm will not make a significant change in the pressure drop. Therefore, it is trivial for the result if further reduce the base size, the 1.0mm base size is sufficient to reproduce the internal fields correctly.
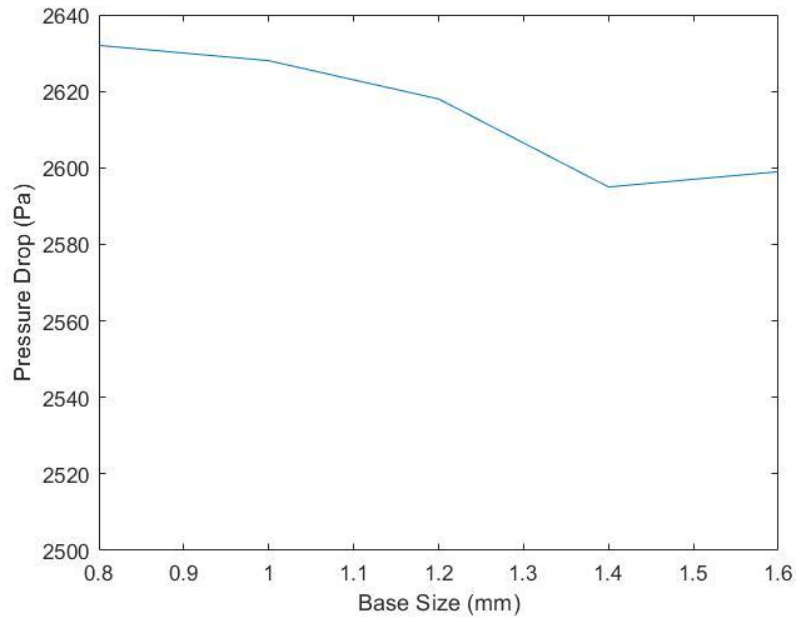
Fig. 7: Pressure Drop vs. Base Size

Next, as shown in Fig. 8, at the fixed base size, as the number of prism layer increases, the pressure increases sharply at the early stage, then decrease gradually, reaching a relative convergence. To make a balance of the computation time and the accuracy, the number of prism layers is set as 5 in this study.
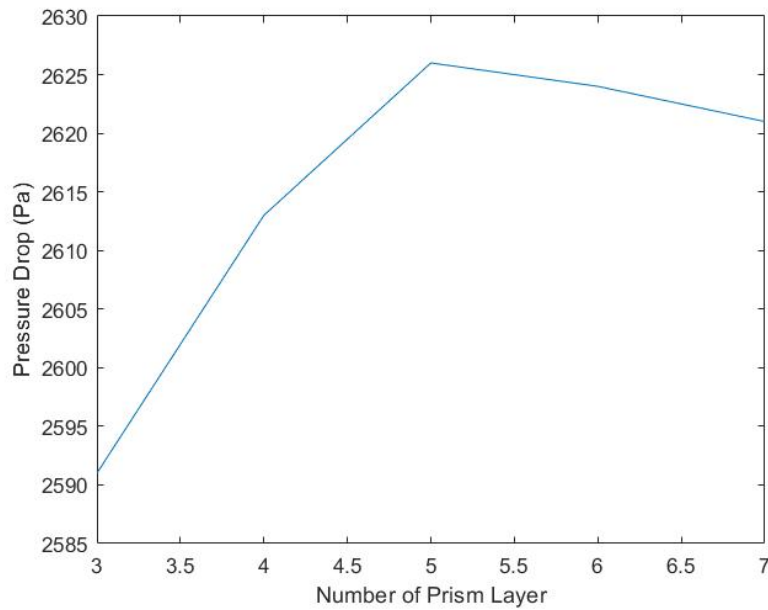

Fig. 8: Pressure Drop vs. Number of Prism Layer

Residuals are important criteria to judge the convergence of the simulation. For the cases finished in this study, the residuals are always less than $1.0×10^{-4}$, the residual values are shown in the figure below.

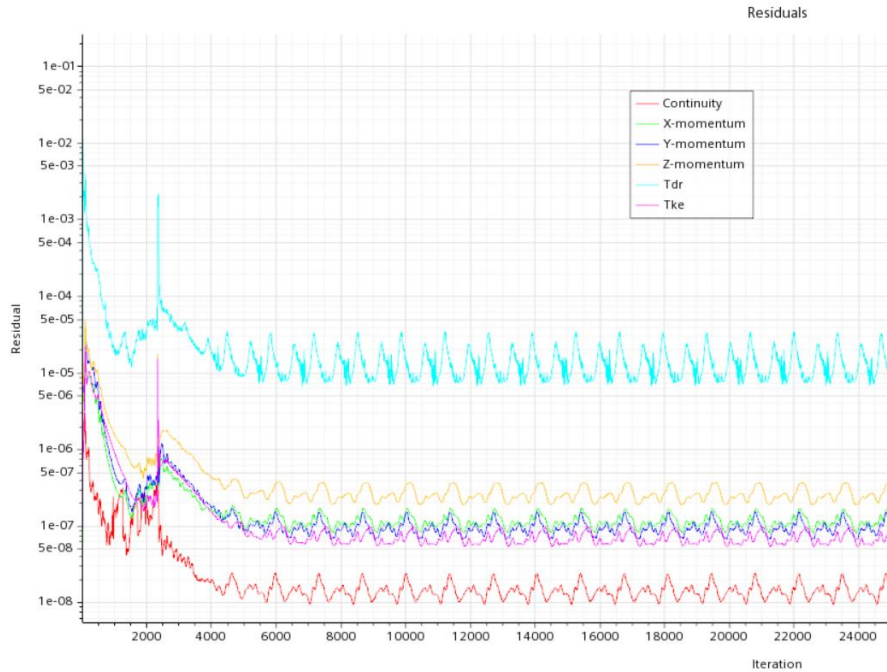Fig. 9: Residuals of Mesh with 1.0 mm Base Size and 5 Prism Layers

4. Results and Discussion

4.1 Pressure Drop

The pressure drop for two models: one with deformation vanes, and the other with non-deformation (closed) vanes were all monitored. Note that both models are non-inclined. As expected, the open vanes introduce a larger flow area, which leads to a lower pressure drop along the channel for the deformation model. Generally, the pressure drop is about 46% lower than that of the model with closed vanes. Meanwhile, by increasing the inlet velocity from 0.5 m/s to 1.5 m/s, it is shown from the tendency that a higher velocity leads to a larger pressure drop along the coolant channel. The outer surface's pressure drop contour with 0.5 m/s inlet velocity (open vanes) is also shown below, it is clear that the pressure value changes dramatically near the controller area.
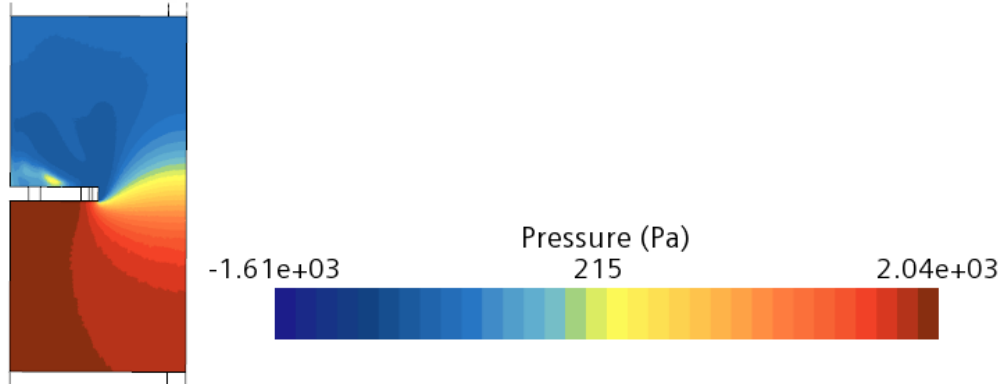
14

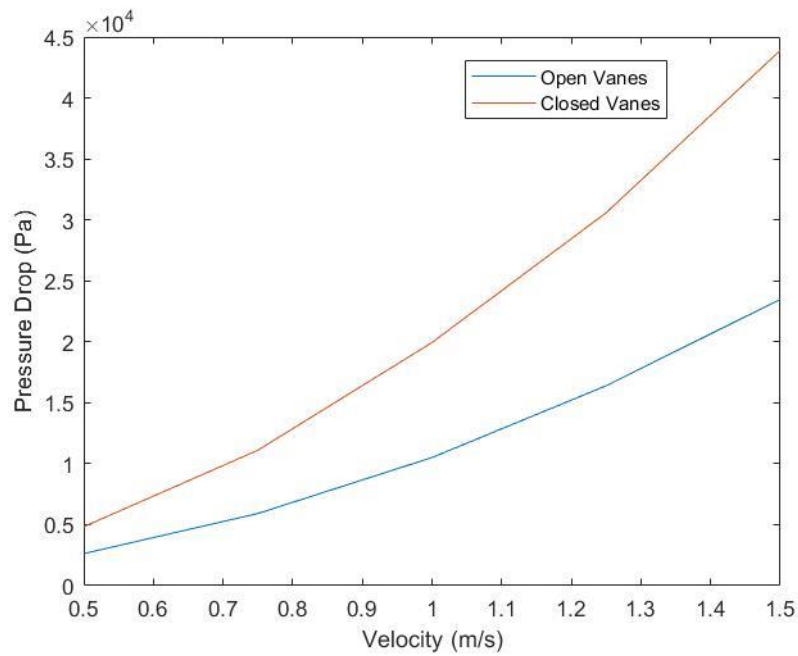Fig. 10: Pressure Contour of the Channel Surface

Fig. 11: Pressure Drop vs. Inlet Velocity with Closed and Open Vanes

A new design of the controller which has an inclined orifice has also been tested with inlet flow velocity also ranging from 0.5 m/s to 1.5 m/s, the results are shown in the figure below. For this inclination model, the shape of the vanes, as well as the radius of the central region, are all the same as the original design, and the inclination angle of the orifice is set as 30° (150°).
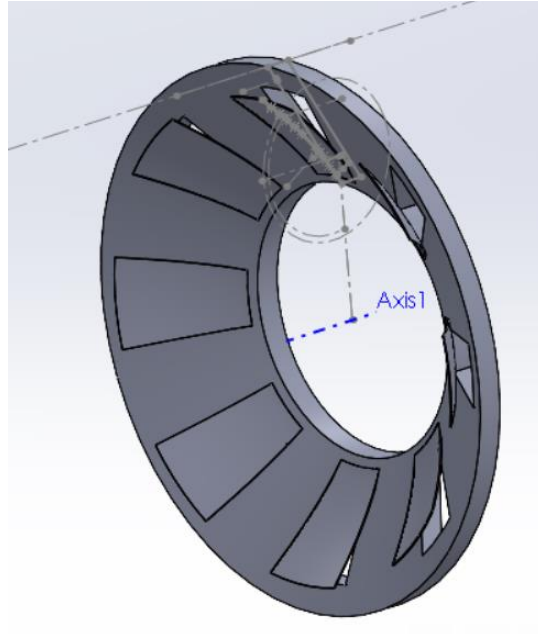
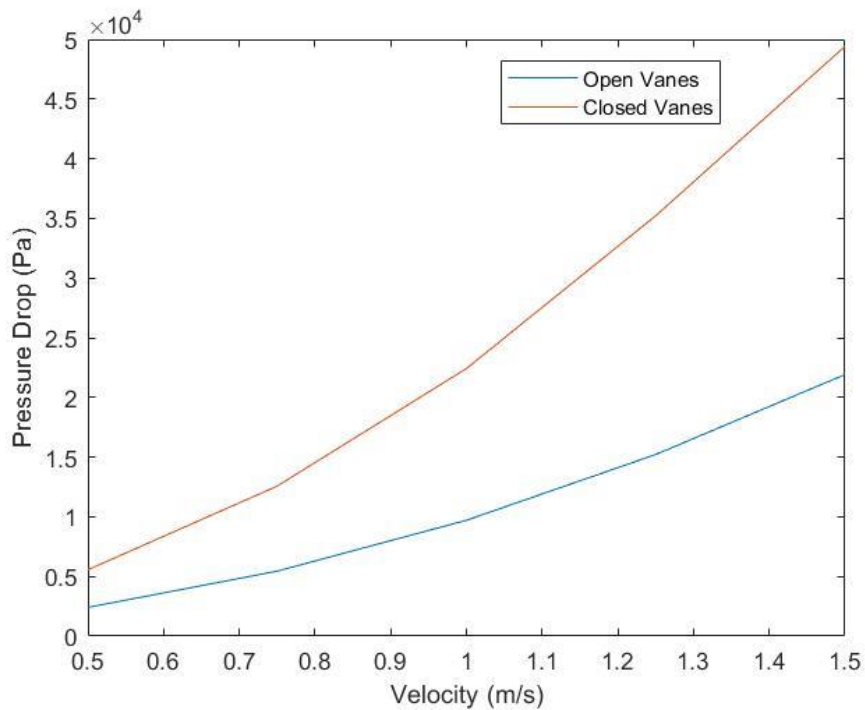Fig. 12: A New Design of Controller with an Inclined Orifice

Fig. 13: Pressure Drop vs. Inlet Velocity with Closed and Open Vanes (with Inclined Orifice)

Per simulation results, the total pressure drop is very close to the value obtained from the previous design. However, slight differences are found that this design has about 10%

lower pressure drop with vanes' open state, and in contrast, around 15% higher pressure drop with vanes closed.

It is also interesting to compare the pressure drop ratio for the two designs mentioned above, note that the pressure drop ratio is defined as the ratio between pressure drop reduction before and after using vanes and the pressure drop values without vanes. The model with an inclined orifice has about 10% larger pressure drop reduction compared to the model with a normal orifice. Therefore, to achieve a higher pressure drop decrease compared with that of the initial model under a fixed inlet velocity, this new design can be taken into consideration.
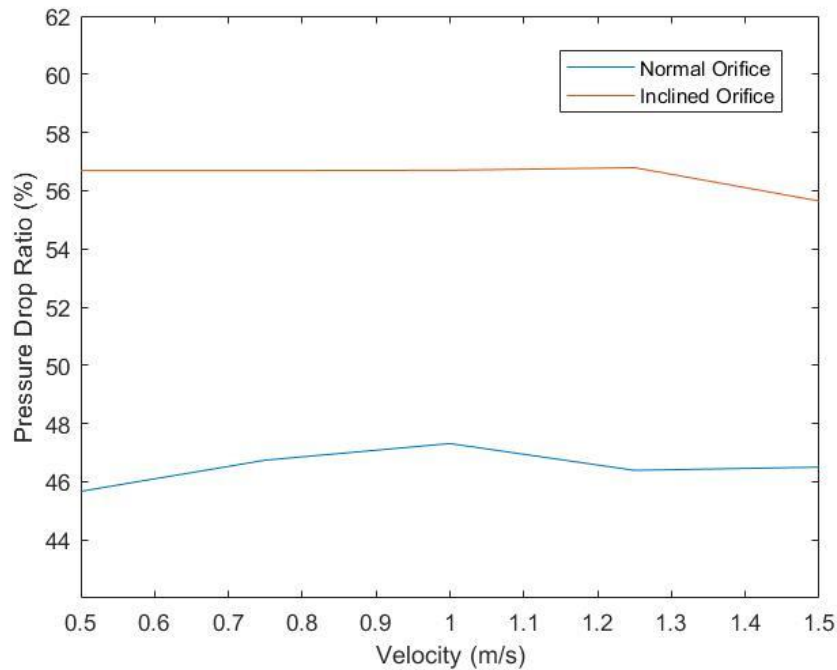

Fig. 14: Pressure Drop Ratios of Two Designs

4.2 Mass Flow Rate

The liquid may also flow through the windows as the vanes open, so it is meaningful to study how much liquid is flowing through the windows and how much is flowing through the center. The simulation results of the mass flow rate through different locations are shown below. The majority of the flow still passes through the center.
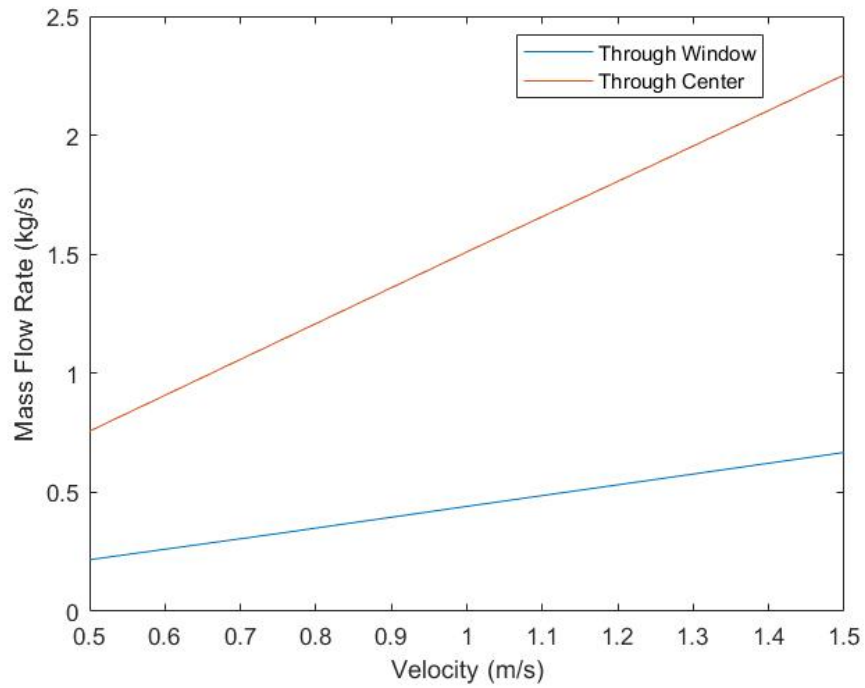
Fig. 15: Mass Flow Rate vs. Inlet Velocity

The results of the mass flow rate ratio are shown in the figure below, which is defined as the ratio between the mass flow rate through the window and the mass flow rate through the center. The mass flow rate ratio increases slightly when increasing the inlet velocity. By increasing the inlet velocity to 3 times, the mass flow rate ratio only increases about 5%. Thus, we can conclude that the mass flow rate ratio is independent of the inlet velocity.
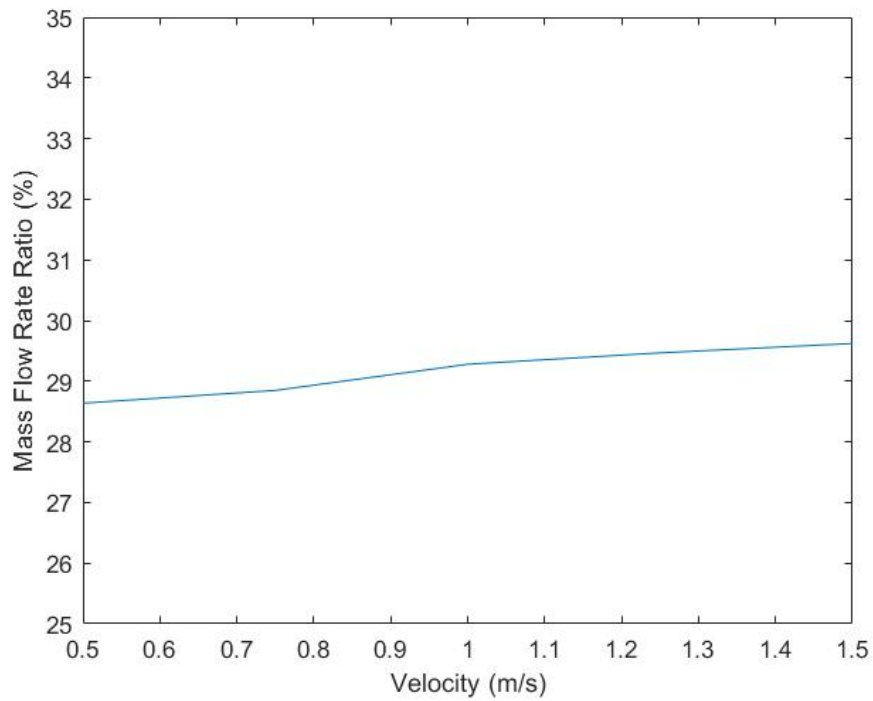
Fig. 16: Mass Flow Rate Ratio vs. Inlet Velocity

4.3 Different Shapes

4.3.1 Change Controller's Inclination Degree

It is proved in Section 4.1 that the inclination degree of the controller will influence the pressure drop value. The inclination degree, originally set as 150° and defined in Fig. 17, can be further reduced until a value close to but not equal to 90°. Additional three models with inclination degrees, 170°, 160°, and 140° are created for further CFD analysis. Note that the shapes of vanes and controller's radius remain the same, the corresponding FEM models are shown in Fig. 18.
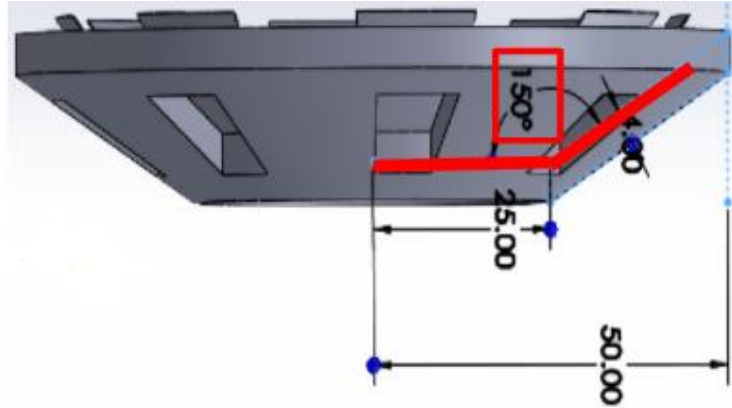
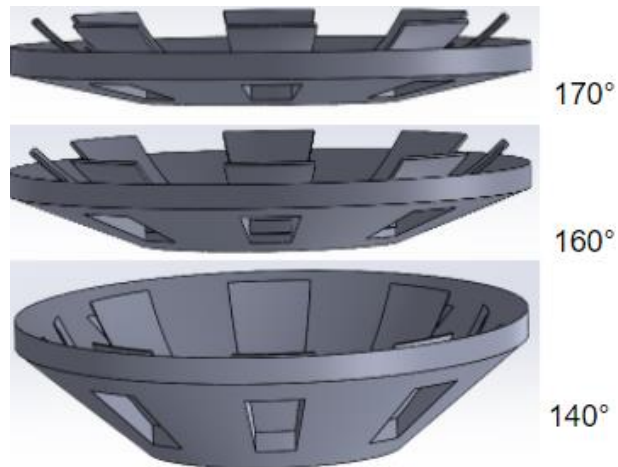Fig. 17: Definition of Controller's Inclination Degree

Fig. 18: FEM Models with Different Inclination Degrees

For this set of the CFD analysis, the inlet velocity is set as 1.5 m/s for all three models. Note that the base size of the mesh is the same as the models generated previously. The pressure drop values are shown in Fig. 19. Same as the conclusion obtained in the previous section, a lower inclination degree can reduce the total pressure drop value, while a variance of 30° can only contribute to approximately 8% pressure drop. To sum up, introducing inclination can reduce the pressure drop, but not much significantly.
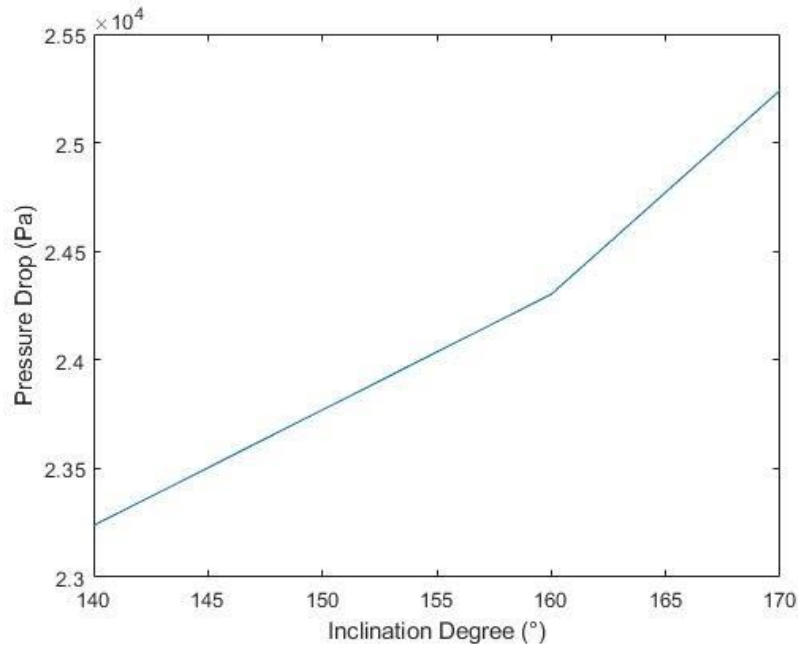
Fig. 19: Pressure Drop vs. Inclination Degree

4.3.2 Rotate Controller for 180°

Another option is simply to reverse the orientation of the controller within the channel for 180°, a comparison diagram is shown in Fig. 20. The shape of these two controllers is the same, while the only difference between the two models is the orientation of the models. Note that based on the definition of the inclination degree in Section 4.3.1, the inclination degrees for those rotation models will be less than 90°.
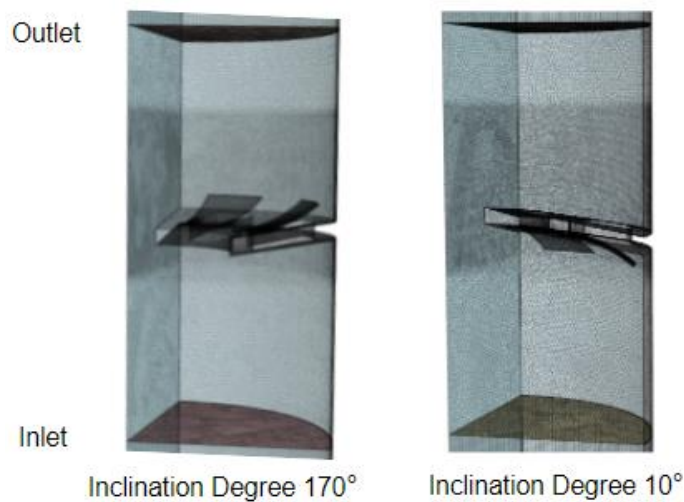

Fig. 20: Comparison Diagram of Models Before and After Rotation

Five inclination degrees, ranging from 0° to 40°, are tested in STAR-CCM+ to monitor the pressure drop values. As shown in Fig. 21, the tendency matches the previous conclusion, while the variance of pressure drop is much more significant compared with the data obtained from non-reversed models.
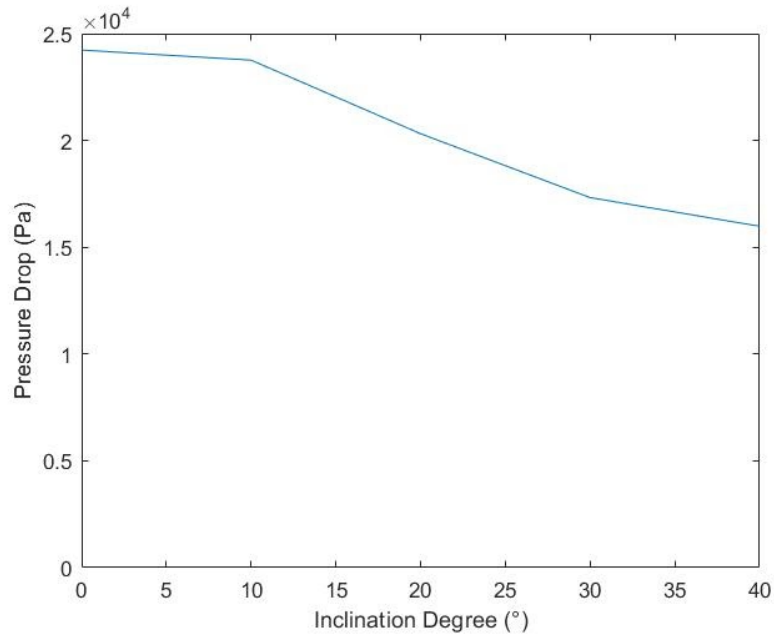

Fig. 21: Pressure Drop vs. Inclination Degree for Reversed Controller Models

Table 4: Comparison of Pressure Drop Before and After Rotation

	Inclination Degree (°)	Pressure Drop (Pa)	Inclination Degree (°)	Pressure Drop (Pa)	Variance
1	140	23237.45	40	15982.50	31.22%
2	160	24302.52	20	20314.86	16.41%
3	170	25241.33	10	23759.55	5.87%

From Table 4 and Fig. 21, by rotating the controller for 180°, the pressure drop will reduce. Furthermore, using a controller after rotation can lead to a much sharper reduction in pressure drop when increasing inclination angle (e.g., a 30° inclination degree variance leads to 7.93% and 32.73% pressure drop variances respectively). Therefore, to obtain a lower pressure drop, it is reasonable to rotate the original orientation of the controller within the channel for 180°. Fig. 22 shows the differences in internal velocity fields between the two models. The velocity distribution near the controller region has a significant variance.
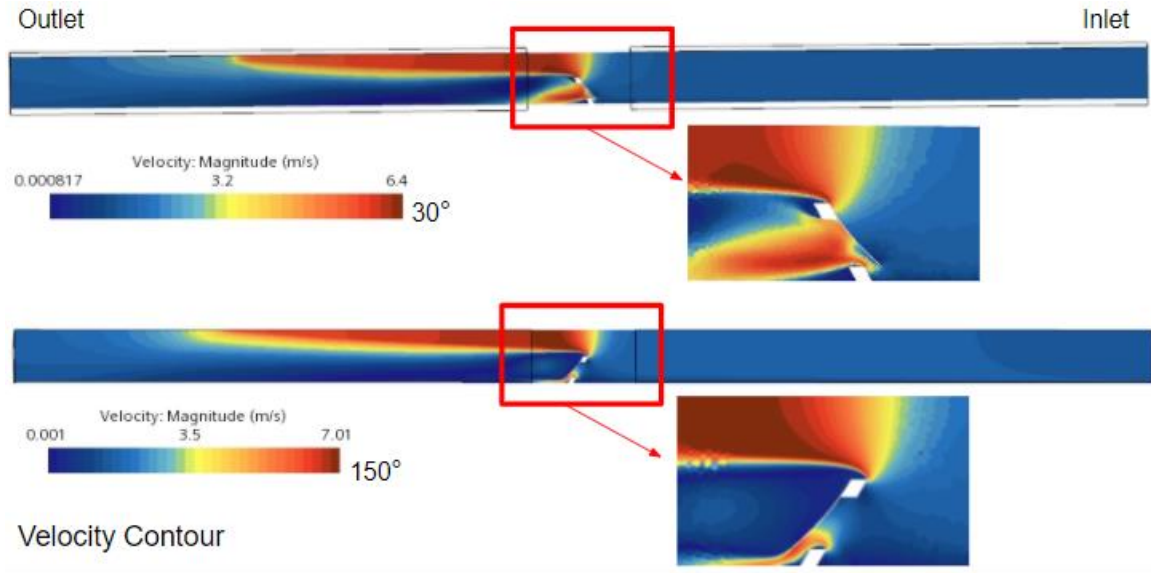
Fig. 22: Difference of Velocity Fields

4.3.3 Rotate Controller for 180°

By swapping the types of the inner and outer material of the bimetallic vanes and changing the contact surface of the controller's ring, one can obtain new controller models that have opposite orientations of vanes' deformation. A sketch of this design is shown in Fig. 23.

Towards Outlet (current)　　　　Towards Inlet (new)
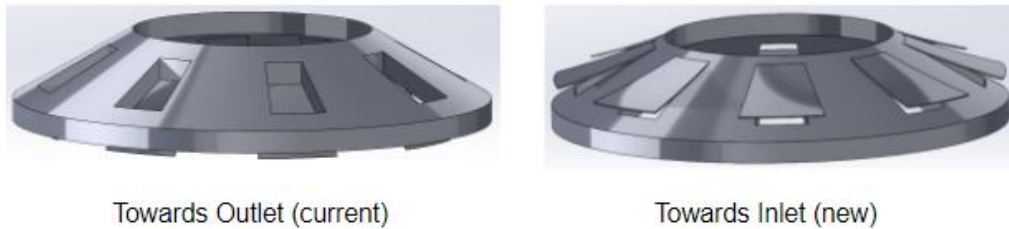
Fig. 23: A New Design with Opposite Orientation of Vanes' Deformation

By testing different inlet velocities and comparing with the initial inclination models, it can be seen that although this new design can reduce the pressure drop by about 46% compared with the non-vanes inclination models, it is still approximately 25% larger than the models with the original vanes deformation orientation. Therefore, this new model cannot contribute to further decreasing the pressure drop.

Fig. 24: Pressure Drop vs. Inlet Velocity for 3 Inclination Models
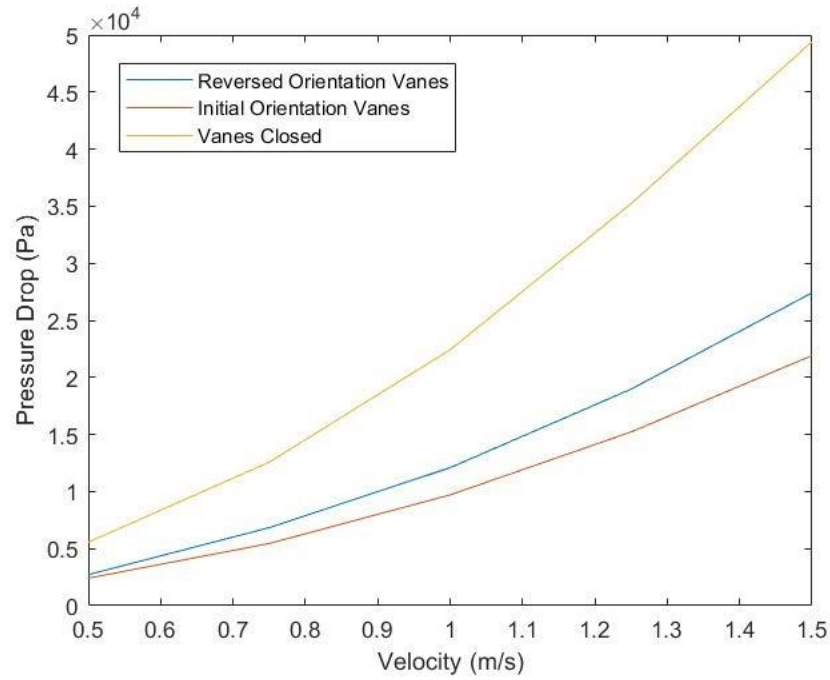
4.3.4 Reverse Vanes

Another design is to have vanes on both sides of the controller (see Fig. 25 and Fig. 26), while the total number of the vanes can be the same or larger.
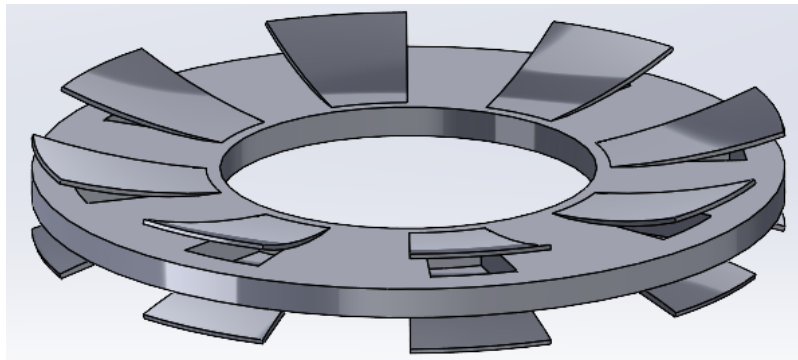

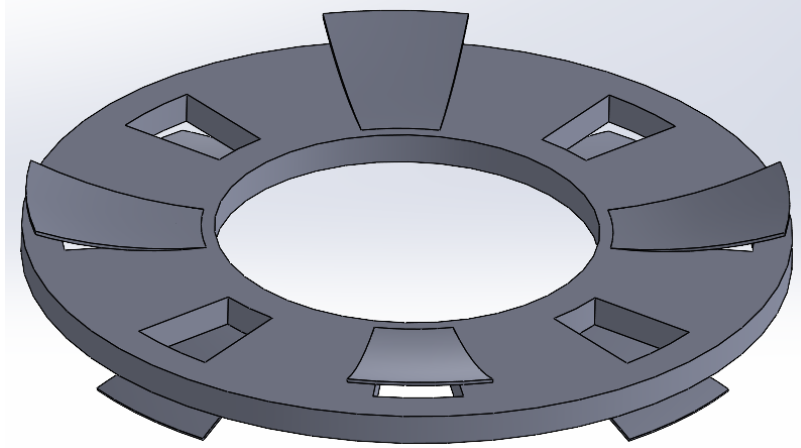Fig. 25: Controller with Vanes on Two Sides (With More Vanes)

Fig. 26: Controller with Vanes on Two Sides (With the Same Number of Vanes)

The simulation results show that these models have worse performance on reducing the pressure drop compared to the original non-inclined model with all vanes at the same side. For instance, for the 1.5 m/s inlet velocity case, the pressure drop of the previously listed two models are 33524.63 Pa and 26888.82 Pa, which are all larger than that of the original model (23487.99 Pa). As shown in the velocity contour of the model with vanes on each window, the two vanes still almost close the local region to let the water flow, this is the main reason why the pressure drop is very high compared with that in other models.

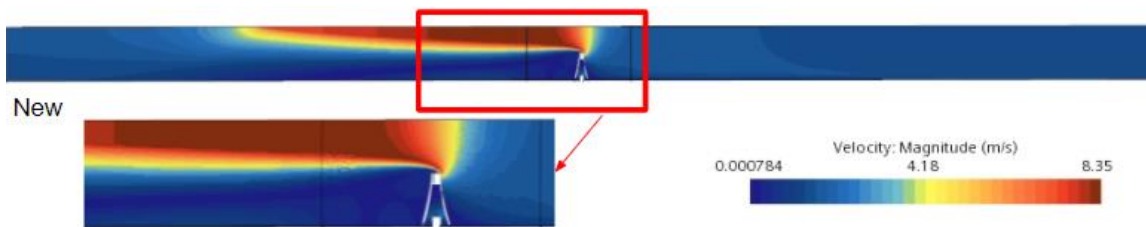Fig. 27: Velocity Contour of the Model with Vanes on Two Sides of the Windows (i.e., Fig. 25)

To allow larger flow areas when temperature increases, another new design is to use two vanes that will deform towards different sides of the controller for each window, while the two vanes are touched at the initial temperature. Note that the width of each vane is 50% of the initial width. The deformation model is shown in Fig. 28.
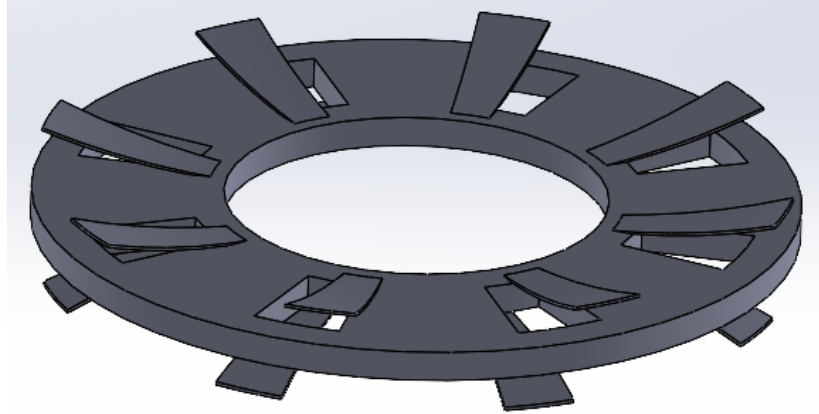
Fig. 28: Controller with Two Vanes Mounted on One Window (Different Sides, Half-Width)

As expected, the simulation results prove that this design can significantly reduce the pressure drop. For instance, the pressure drop for the 1.5 m/s inlet velocity is only 20915.85 Pa, which is 10.95% smaller than the original model. The corresponding velocity contour is shown in Fig. 29, note that the thickness of the controller will influence the simulation result greatly for this model since eight windows have already existed at the initial temperature. Additional studies using different controller thicknesses are needed to verify the influence of the thickness.
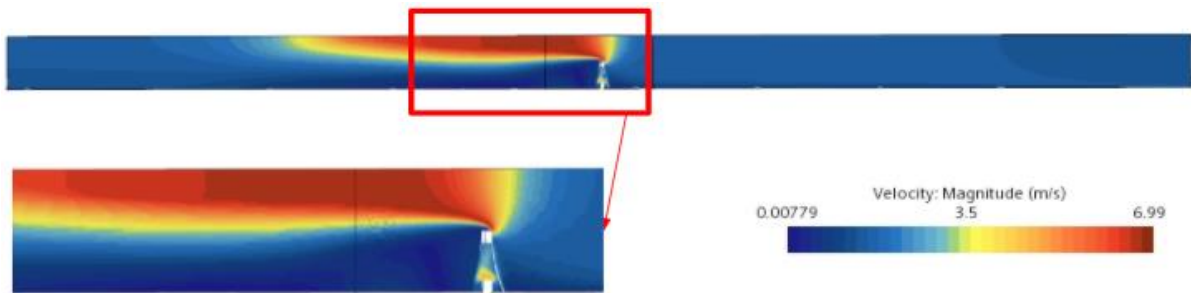

Fig. 29: Velocity Contour of the Model with Vanes on Two Sides of the Windows and Half-Width (i.e., Fig. 28)

5. Conclusion

It has been found in this project that Invar has extraordinary properties to be used in the bimetallic material study, including its low thermal expansion coefficient, and high stability, etc. The corresponding Invar-Stainless Steel material pair FEM deformation

models are created and imported into STAR CCM+ to perform detailed CFD simulations. It has been concluded from the simulation results that the channel with open vanes inside can sharply reduce the total pressure drop along the pipe and increase the total mass flow rate which is flowing through the vane-deformed-generated windows. It has also been found that increasing the inlet velocity of the flow can roughly proportionally increase the total pressure drop. Furthermore, new design models that have inclined orifices have also been studied and the simulation results are used to compare with the current version of the design. For example, different inclination models with various inclination degrees, vanes deformation orientations, and rotation, etc. are tested and prove that reversing the controller can significantly reduce the pressure drop value, while the other two options have little or even negative impact on reducing pressure drop. Compared with the existing actively controlled valve design, this passively controlled system only relies on the basic physical characteristics of the materials, which brings relatively higher reliability. In sum, the obtained results of this study are encouraging, which proves the applicability of using different designs of the passively controlled valves to adjust the water flow and heat transfer within the channels, and finally achieves the purpose of finer reactivity control, which is also of great importance in the design of the nuclear reactor.

Reference

[1] Pattison R C, Donahue M M, Gupta A M, et al. Localized temperature control in microchannel reactors using bimetallic thermally-actuated valves[J]. Industrial & Engineering Chemistry Research, 2015, 54(24): 6355-6361.

[2] Verstraete T, Li J. Multi-objective optimization of a U-bend for minimal pressure loss and maximal heat transfer performance in internal cooling channels[C]//Turbo Expo: Power for Land, Sea, and Air. American Society of Mechanical Engineers, 2013, 55140: V03AT12A041.

[3] Boughaleb J, Arnaud A, Guiffard B, et al. Coupling of PZT thin films with bimetallic strip heat engines for thermal energy harvesting[J]. Sensors, 2018, 18(6): 1859.

[4] Boisseau S, Despesse G, Monfray S, et al. Semi-flexible bimetal-based thermal energy harvesters[J]. Smart Materials and Structures, 2013, 22(2): 025021.

[5] Park C W, Kim H Y. A Study on the Auto-mobile Gas Spring Structural Analysis Using of Bimetal[J]. Journal of the Korean Society of Manufacturing Technology Engineers, 2013, 22(1): 131-137.

[6] Manesh D, Taheri K. An investigation of deformation behavior and bonding strength of bimetal strip during rolling[J]. Mechanics of Materials, 2005, 37(5): 531-542.

[7] Shi X, Yang F, Xu S, et al. A passive temperature-sensing antenna based on a bimetal strip coil[J]. Sensors, 2017, 17(4): 665.

[8] Kawase Y, Ichihashi T, Ito S. Heat analysis of thermal overload relays using 3-D finite element method[J]. IEEE transactions on magnetics, 1999, 35(3): 1658-1661.

[9] Chevalier J, Olagnon C, Fantozzi G, et al. Creep behaviour of alumina, zirconia and zirconia-toughened alumina[J]. Journal of the European Ceramic Society, 1997, 17(6): 859-864.

[10] Agbodemegbe V Y, Cheng X, Akaho E H K, et al. An investigation of the effect of split-type mixing vane on extent of crossflow between subchannels through the fuel rod gaps[J]. Annals of Nuclear Energy, 2016, 88: 174-185.

[11] Arnaud A, Boughaleb J, Monfray S, et al. Thermo-mechanical efficiency of the bimetallic strip heat engine at the macro-scale and micro-scale[J]. Journal of Micromechanics and Microengineering, 2015, 25(10): 104003.

[12] Hsu Y J, Chang Y H, Chai Y L, et al. The influence of residual stress and membrane thickness on the performance of Fe–Ni–Cr/Invar bimetal freestanding membrane for microdevices[J]. Sensors and Actuators A: Physical, 2002, 101(1-2): 160-167.

[13] Panowicz R, Kucewicz M. Numerical analysis of temperature influence on deformation and effort of bimetallic element[J]. Journal of KONES, 2016, 23.

[14] Kumar R K J, Ashokkumar T, Sivakumar P. Comparative analysis of deflection in a bimetal[C]//IOP Conference Series: Materials Science and Engineering. IOP Publishing, 2021, 1091(1): 012070.

[15] Van der Schaaf B. The effect of neutron irradiation on the fatigue and fatigue-creep behaviour of structural material[J]. Journal of Nuclear Materials, 1988, 155: 156-163.

[16] Khan M T. STUDY OF THERMAL DEFORMATION ANALYSIS IN AL-STEEL AND CU-STEEL BIMETAL COMPOSITES BY ANSYS STATIC STRUCTURAL[J]. 2021.

APPENDIX B

20th International Topical Meeting on Nuclear Reactor Thermal Hydraulics (NURETH-20) Summary

Passive temperature-sensitive flow-controlling device based on bimetallic membrane deflection, FEM, and CFD feasibility study

Victor Petrov[1,2,3], Yucan Ding[1,2]

[1] Department of Nuclear Engineering & Radiological Sciences, University of Michigan–
Ann Arbor, MI, USA

[2] ETH Zurich, Department of Mechanical and Process Engineering, Sonneggstrasse 3, 8092, Zurich,
Switzerland

[3] Laboratory for Reactor Physics and Thermal-Hydraulics (LRT), Paul Scherrer Institut, 5232 Villigen
PSI,
Switzerland

petrov@umich.edu, yucan.ding@psi.ch ;
*[leave space for DOI, which will be inserted by ANS]*

ABSTRACT

Passive flow control devices could be utilized in various parts of a power plant installation, for instance, to throttle the flow through temperature-sensitive elements to avoid overheating, redirect flow to heat exchangers, etc. This work shows a feasibility analysis for applications of novel bimetallic flow controllers of various geometries and their potential performance. Even though the application of bimetallic materials is not new and widely used in the automotive industry and in electromechanical devices, its application in the nuclear field is limited and usually restricted to the actuation of mechanical components. The present study includes final element modeling (FEM) to evaluate bimetallic membranes deflection for multiple materials, shapes, thicknesses, and CFD simulations for various flow controller shapes and configurations, aimed at the optimization of the device geometry from a flow control capabilities standpoint. The flow control capabilities were evaluated based on the pressure drop across the fully open and fully closed device for different fluid mass flowrate and temperatures. Preliminary results show a good device candidate that allows to reach up to three times in pressure drop difference between fully closed and fully open devices.

KEYWORDS
Passive flow controller, CFD, FEM, bimetallic

1. INTRODUCTION

Bimetallic strips were invented by clockmaker John Harrison in the 1750s as a way to counter the impact of temperature on H3 marine timekeepers [1]. The principle behind their operation is based on the mechanical coupling of two strips of metal with differing coefficients of thermal expansion. When subjected to a temperature change, the bimetallic strip will deform in the direction of the metal with the lower coefficient of thermal expansion as shown in **Figure 1**.
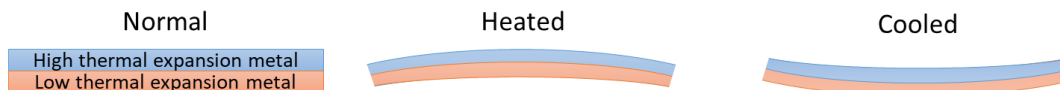

Figure 1: Working principle

The phenomenon of bimetallic strips is currently utilized in a wide range of devices and industries, including temperature sensing, thermal actuators, temperature-dependent switches, electrical current limiters, and many others. These devices can be found in a variety of sectors, including automotive, electromechanical, medical, aerospace and beyond [2,3,4]. Recently, bimetallic strips have also been used in the field of renewable energy generation as a means of harvesting thermal energy in the form of a thermal motor[5]. Furthermore, some authors investigated application of bimetallic actuated valves for local temperature control in microchannel chemical reactors [6] or to enhance heat transfer using adaptive bimetallic fins [7]. It was noted the publicly available literature contains quite a several publications utilizing FEM methods to evaluate bimetallic stripe deformations for different materials in different temperature ranges, which agrees well with analytical models or experimental investigations[8,9,10].

To date, there is no reported use of bimetallic systems with significantly different coefficients of thermal expansion in the nuclear industry. However, other types of bimetallic systems have been utilized in nuclear engineering. For example, bimetallic pipes made of two layers of metal with different corrosion resistance properties have been studied and implemented[11]. The use of these pipes allows for the creation of piping with enhanced corrosion resistance using less metal. The application of bimetallic pipes in nuclear power plants has also led to research into methods for bonding various metals together which might benefit the reported study as well [12,13].

The purpose of this study is to investigate the potential use of bimetallic strips in the passive control of nuclear power plants during different operating regimes. To achieve this goal, a novel flow controller incorporating bimetallic vanes within the coolant piping system was designed and tested. The controller was able to adjust the pressure drop (friction factors) as a function of coolant temperature, allowing for load-following by increasing or decreasing the flow of coolant in designated areas through the deformation of the bimetallic vanes in response to changes in temperature. The use of bimetallic strips for passive flow control in load-following nuclear microreactors was originally proposed for the Holos-Quad microreactor developed by HolosGen LLC. Detailed load following analysis of the Holos-Quad microreactor was performed by ANL and HolosGen within an ARPA-E MEITNER program and reported in [14,15]. Where five reactor control mechanisms were reported with associated cycle efficiency: turbine bypass, turbine throttling, compressor throttling, inventory, and compressor speed, some of which could be used with the proposed bimetallic-based flow controller.

The flow controller consists of U-shaped bimetallic vanes mounted on the ring in the flow control duct with machined apertures, inner duct diameter (ID) assumed to be 100mm, and flow controller geometry is shown in Figure 2. When the flow temperature exceeds a predetermined setpoint, the bimetallic vanes will deform in a controlled manner, opening additional flow windows. This increases the flow area, reducing the pressure drop across the flow controller and enabling more coolant to flow. The flow controller can be used to either enhance heat removal or redirect coolant towards auxiliary systems.
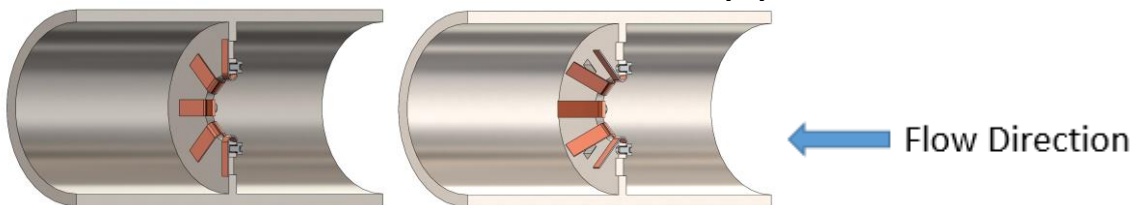

Figure 2: Bimetallic flow controller. Closed state (left), open state (right).

In order to evaluate the feasibility of the proposed approach, detailed FEM analyses of the bimetallic strips of different material compositions for assessing achievable vane deformation and CFD analyses of fully open flow controllers at different coolant flowrates to estimate possible pressure drop reduction between fully open and fully closed flow controller states.

2. Bimetallic strip material selection and deformation analyses using FEM methods.

There are several approaches reported in the literature to estimate bimetallic strip bending (deformation) as a function of stripe thickness, length, and material properties, e.g., thermo-expansion and Young's modulus at different temperature conditions [8,9,10], however the application of such methods for nonregular shapes and multiplane bending might pose some difficulties. Hence it has been decided to utilize FEM simulation tools such as Solidworks simulation (for rough deformation estimation) and ANSYS for higher fidelity deformation conformation[16, 17].
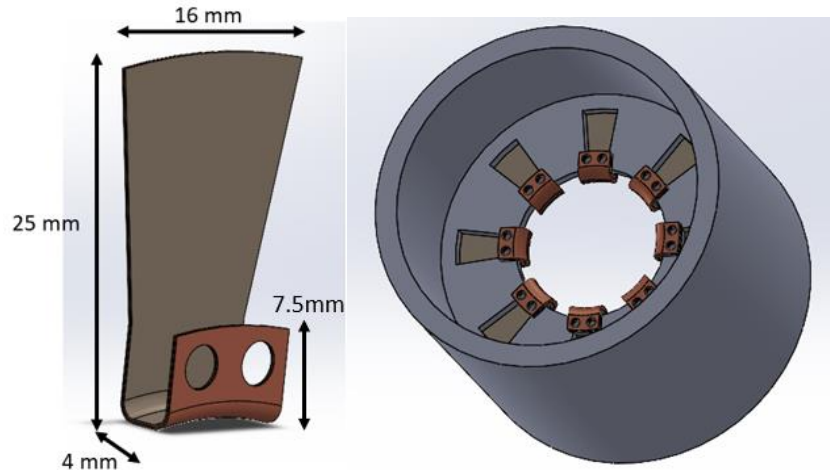
Figure 3: Sketch of Non-deformed bimetallic vane (left) and assembled flow controller (right).

The bimetallic vanes used in this study are designed with a U-shape to maximize deformation and have an inner layer with a higher coefficient of thermal expansion. This allows maximizing vanes bend away from the ring. Vane is mounted on the opposite side of the flow controller ring using a screw (see Figure 3). At the initial temperature, the vane is not deformed and fully closes the apertures in the ring.

In the selection of materials for the bimetallic vanes, it is important to consider the properties of the flowing media from a corrosion resistance perspective, as well as the effects of neutron and gamma radiation exposure and temperature fluctuations on material fatigue. These factors are especially critical for bonding between different metals in the bimetallic strip. However, at this stage of the study, we are only verifying the general feasibility of the proposed flow controller without a specific installation location. Therefore, the initial material selection is primarily based on the coefficient of thermal expansion.

In the present study, we selected the nickel-iron alloy FeNi36, also known as "Invar," for all performed analyses. This alloy has a very low coefficient of thermal expansion $1.2 \times 10^{-6} K^{-1}$ which remains almost constant in a wide range of temperatures up to 500 K and also exhibits good fabrication properties including ductility and toughness [18]. In addition, parts made of Invar alloy can be successfully manufactured using wire-arc additive manufacturing methods without defects such as pores, cracks, or lack of fusion. This fact may be important for the fabrication of parts in the future [19]. In the material selection process, various materials were considered for the inner vane layer. The properties of these materials, including their thermal expansion coefficients and maximum displacements, are summarized in Table 1. Ultimately, stainless steel was chosen for use in the further analysis due to its satisfactory corrosion resistance compared to copper, as well as its adequate displacement compared to titanium alloy and ductile iron.

Table 1 Inner layer materials

| Material	Coefficient of Thermal Expansion (1/K)	Maximum Displacement (mm)
Copper	2.4×10^{-5}	10.32
Titanium Ti-8Al-1Mo-1V	8.0×10^{-6}	2.99
Ductile Iron	1.1×10^{-5}	4.14
Stainless Steel (ferritic)	1.1×10^{-5}	5.44

Initially, it was planned to use Solidworks Finite Element Method (FEM) simulation capabilities to predict vane deformation under heat exposure. Preliminary simulations using relatively thick samples (10mm) demonstrated good agreement with theoretical curves, with a difference of within 3%. The accuracy of these simulations was also confirmed by the SOLIDWORKS Simulation Validation report[20]. However, when the vane thickness was reduced below 1mm, it became difficult to achieve good control over the computational mesh, making it challenging to verify mesh sensitivity. As a result, further FEM analyses were conducted using ANSYS. A sample of the FEM mesh of a single vane is shown on Figure 4.
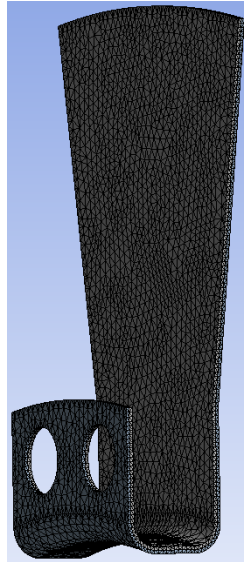

Figure 4: Vane FEM mesh example

A mesh sensitivity study was conducted using a 0.3mm thick vane made of Invar and ferritic stainless steel, which was heated from 50°C to 280°C. The results indicated that the deflection of the vane was relatively independent of the mesh size once the azimuthal size of the mesh elements was reduced below 0.4-0.5mm (see Figure 5 (left)). However, the stress results still showed some variance, even though they did not appear to be sensitive to the actual computational mesh element size (see Figure 5 (right)). Therefore, the results obtained with an element size of 0.4mm can be considered mesh-independent and can be used to obtain the deformed shape of the vane for further computational fluid dynamics (CFD) analyses. The final state of the vane simulated with 0.4mm mesh elements is shown in Figure 6. In addition, a wide range of vanes thicknesses was studied to acquire detection values as a function of vane thickness, obtained results reported in Figure 7.
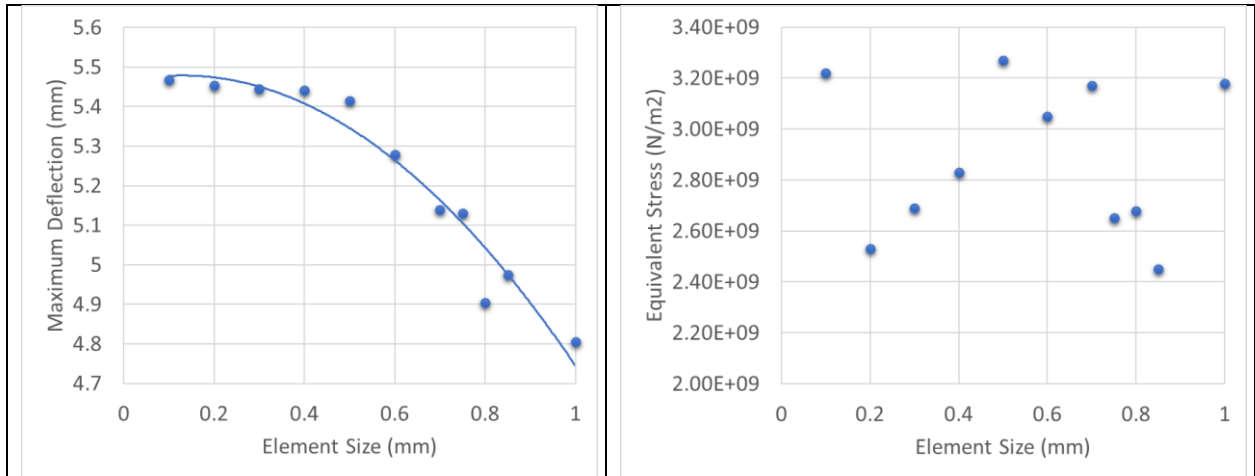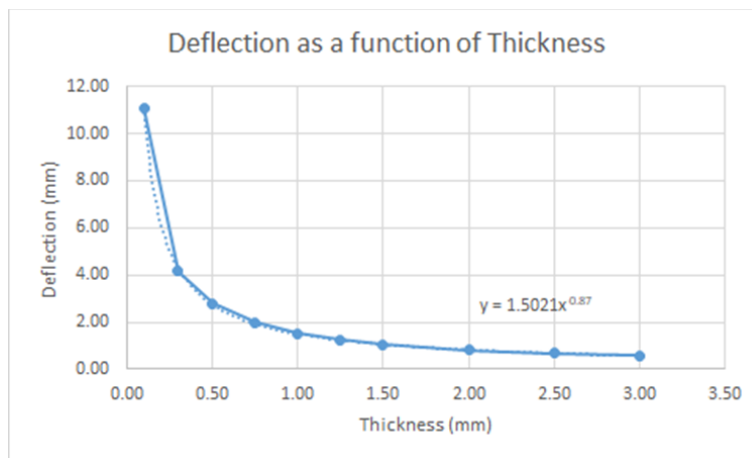
Figure 5: FEM mesh sensitivity of maximum deflection (left) and maximum stress (right).
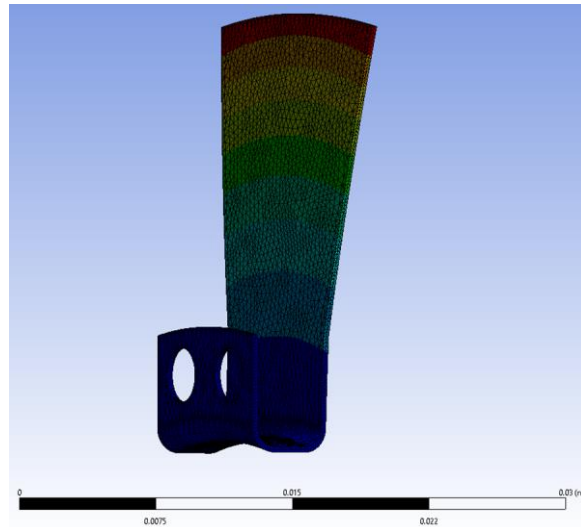
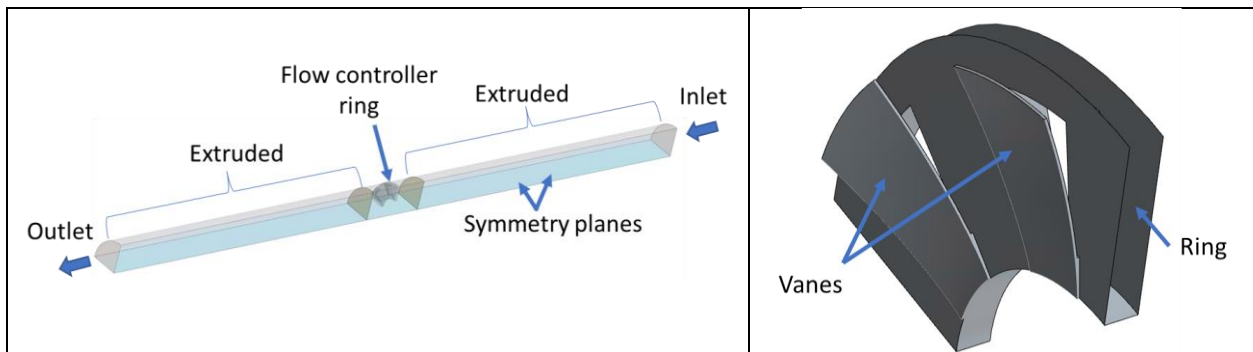**Figure 6: Deformed flow controller vane.**

Figure 7: Maximum deflection vs. vane thickness.

3. Flow controller analysis using CFD methods.

### 3.1. CFD simulation setup

The deformed vane profile obtained from the FEM simulation was imported into the flow controller CAD geometry and attached to the flow controller ring. Several simplifications were implemented to simplify the geometry and meshing, including the omission of the U-shaped mounting parts and screws, as their contributions were considered negligible at this stage. Only the main part of the vane that closes the ring slots was considered in the CFD analysis. All CFD simulations were conducted using Siemens Simcenter STAR-CCM+ 2021.2. The performance of the flow controller was evaluated based on the pressure drop ratio for fully open and fully closed vanes for a range of flow velocities from 0.5 m/s to 1.5 m/s at the inlet of the simulated domain and with a pressure boundary condition at the outlet of the coolant, where the coolant type is water. The length of the entire domain was 1.1m upstream, and the downstream sections were meshed using extrusion. The inlet velocity was set as a uniform for the entire inlet section. While this may not guarantee fully developed flow at the flow controller, it can still be considered a reasonable assumption as it is uncommon for pipes in power plants to run straight for several diameters. Furthermore, we are only estimating the relative pressure difference between the open and closed devices. In future work, verifying the performance under actual flow conditions will be necessary. A quarter symmetry was utilized in order to reduce the computation burden. Flow domain schematic and flow controller detalization used in CFD simulations are shown in Figure 8, the maximum deflection, in this case, is 5.45mm.

Figure 8: Flow controller CFD domain (left) and zoomed controller ring with bimetallic vanes (right).

Simulations were conducted using the realizable k-eps two-layer turbulence model. A CFD mesh sensitivity study was performed at a velocity of 1.5 m/s. The meshed region was divided into two parts, with base-size cells in the periphery and four times finer cells in proximity to the flow controller, as indicated in Figure 9. "Five different base sizes were evaluated. The tested base sizes, corresponding final domain sizes, and pressure drop variations are summarized in Table 2. It should be noted that a two-fold reduction in the base size leads to a five-fold increase in the computational mesh. Despite the maximum pressure drop difference between the tested meshes being only 1.46%, we decided to continue the simulations using the second smallest base size of 1.0mm. Additionally, the sensitivity of the mesh was tested with respect to the number of prism layers, with five options tested using 3, 4, 5, 6, and 7 prism layers. The maximum pressure drop difference was evaluated as approximately 1.4%. All further simulations were performed using five prism layers.
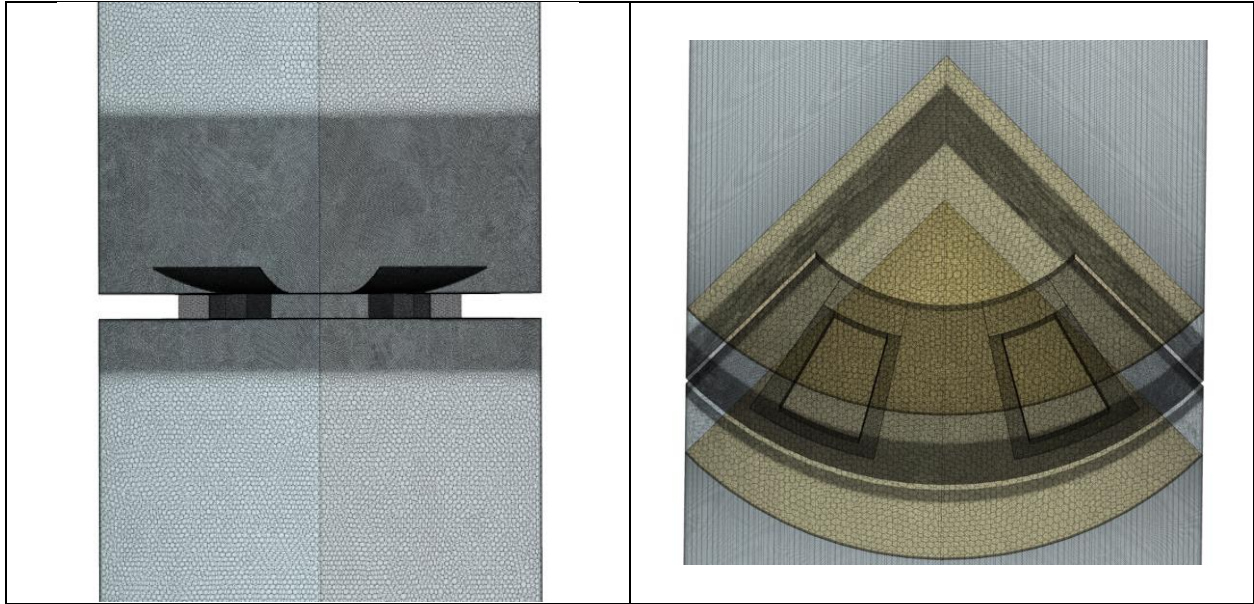
Figure 9: Computation mesh in proximity to the flow controller.

Table 2 CFD mesh sensitivity study

Base size (mm)	Number of Cells (mln)	Pressure drop change (%)
0.8	8.96	0.00
1.0	5.27	-0.16
1.2	3.43	-0.52
1.4	2.40	-1.42
1.6	1.76	-1.26

3.2. CFD simulation results

Simulation results for the baseline flow controller geometry are presented in Figure 10. The Figure 10 (left) shows the pressure drop as a function of inlet flow velocity for two cases with fully open and fully closed vanes. Notably, it can be observed that the pressure drop ratio between the open and closed vane scenarios varies very little over the entire range of examined inlet velocities. The controller with fully open vanes offers approximately 46% pressure drop reduction with respect to fully closed vanes. In addition to the pressure drop, we have found out that in the case of fully open vanes around 30% of the mass flow goes through the slots in the controller ring as it is indicated in Figure 10 (right). A more detailed understanding of the flow field within the flow controller can be obtained from Figure 11 (left). The figure shows how the flow passes through the slot and is redirected by the vanes, resulting in the formation of a recirculation region, as indicated by the streamlines. Figure 11(right) shows the same area in the form of 2D planes for better understanding.
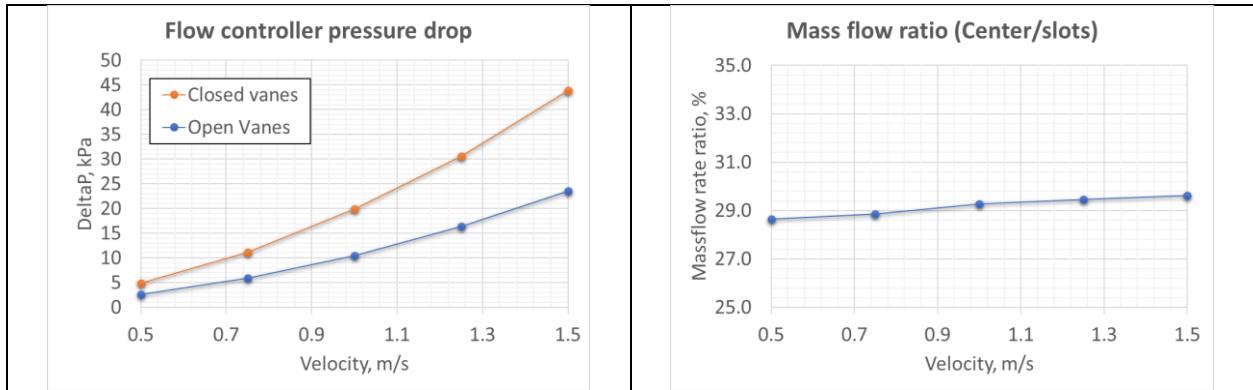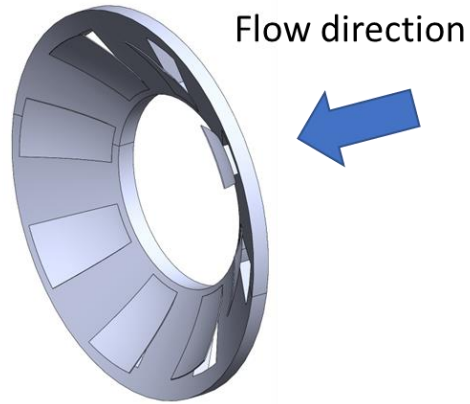
Figure 10: Flow simulation results, pressure drop across the flow controller (left), mass flow ratio for center aperture vs. ring slots (right).
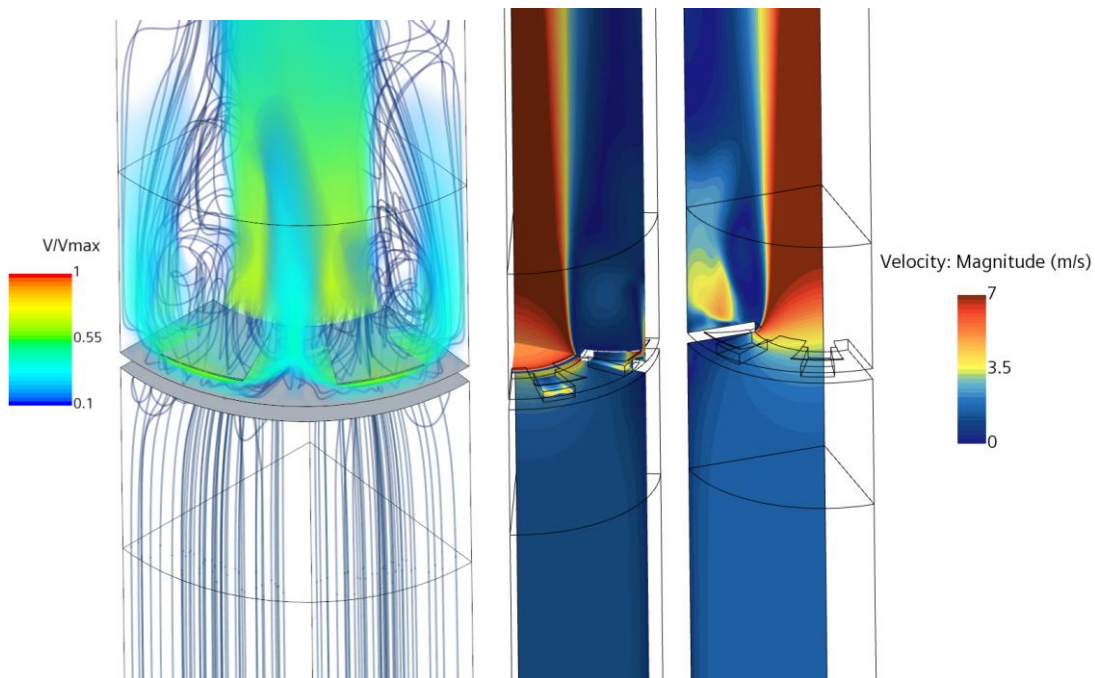

Figure 11: 3D rendering of the flow field and associated streamlines within the flow controller (left) and velocity magnitude in the middle-vanes and between vane sections (right).

To achieve a larger pressure drop ratio, a flow controller with a modified ring geometry was simulated. The ring was inclined towards the inlet for 30deg, while maintaining the same diameter for the central aperture as before as shown in Figure 12. This shape provides a more direct path for the slot flow when the vanes are open, but will also result in a higher pressure drop when the slots are closed. Simulation results shown in **Figure 13** indicates that the pressure drop in fully closed conditions increased by approximately 10%-14% compared to the previous geometry with closed vanes. However, in the case of fully open vanes, the absolute pressure drop was reduced by 7%-9% compared to the previous geometry. And after geometry modification, the controller with fully open vanes offers approximately 56% pressure drop reduction with respect to fully closed vanes. That is ~1.22 higher controllability with respect to the previous geometry. The overall flow field in the controller region (**Figure 14**) is very similar to the previously simulated geometry **Figure 11**(right), except for the reduced size of high-velocity regions between vanes that could speak of more uniform flow.

Figure 12: Modified flow controller geometry.
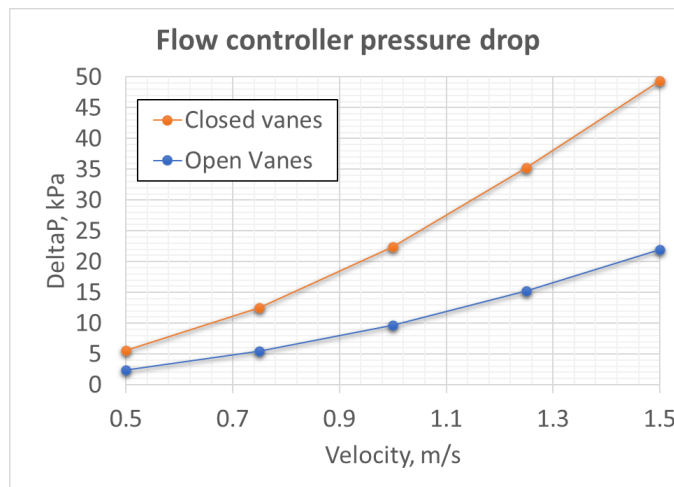
Figure 13: Flow simulation results, pressure drop across modified flow controller
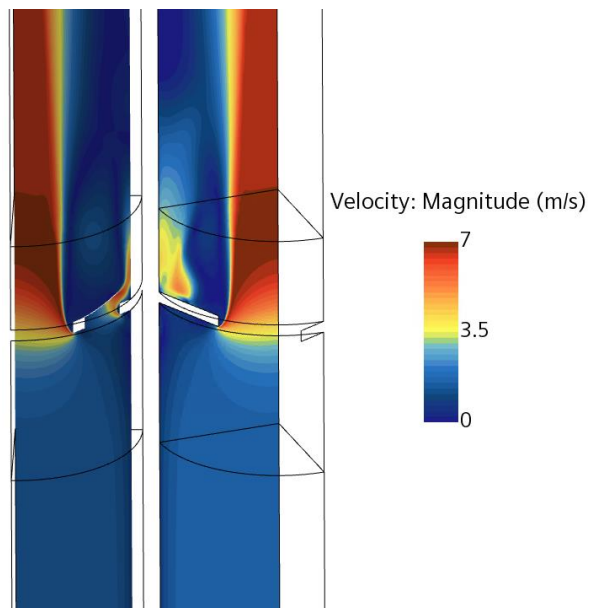
Figure 14: velocity magnitude in the middle-vanes and between vane sections

4. CONCLUSIONS

In summary, this study presents a new device based on bimetallic strip deformation that could be used as a passive flow controller for fluid flow redirection or flow reduction based on the temperature of the flowing media in various regions of power plant piping systems. The feasibility of the device was explored through CFD and FEM simulations, which demonstrated that such a simple device geometry can offer up to 46%-56% pressure drop change, depending on the selected geometry and temperature in a wide range of flow velocities. It should be noted that the proposed geometries are conceptual studies and not final designs, and careful consideration should be given to material selection to ensure good corrosion resistance in the intended flow media and operating conditions. Additionally, measures should be taken to prevent electrochemical corrosion at the bonding layer of the bimetallic strip or at the interface, such as the use of thin buffer layers or encapsulating strips.

ACKNOWLEDGMENTS

REFERENCES

1. Britannica, The Editors of Encyclopaedia. "John Harrison". Encyclopedia Britannica, 20 Mar. 2022, https://www.britannica.com/biography/John-Harrison-British-horologist. Accessed 4 January 2023.
2. Parne Saidi Reddy, R.L.N. Sai Prasad, Dipankar Sengupta, et al. Method for enhancing and controlling temperature sensitivity of fiber Bragg grating sensor based on two bimetallic strips IEEE Photon. J., 4 (2012), pp. 1035-1041, 10.1109/JPHOT.2012.2202102
3. Shi, X.; Yang, F.; Xu, S.; Li, M. A Passive Temperature-Sensing Antenna Based on a Bimetal Strip Coil. Sensors 2017, 17, 665. https://doi.org/10.3390/s17040665
4. Angel, G. D. (2014). Optimisation and characterization of a curved bimetallic blade and its performance within a thermal motor. University of Hertfordshire School of Engineering and Technology, England.
5. Angel, G. 2013. A Sustainable Energy Harvesting Machine, London, IAENG. Proceedings of the World Congress on Engineering 2013 Vol III, WCE 2013, July 3 - 5, 2013, London, U.K. pp2103-2108 ISBN: 978-988-19252-9-9, ISSN: 2078-0958 (Print); ISSN: 2078-0966 (Online)
6. Pattison R C, Donahue M M, Gupta A M, et al. Localized temperature control in microchannel reactors using bimetallic thermally-actuated valves[J]. Industrial & Engineering Chemistry Research, 2015, 54(24): 6355-6361.
7. M. Vilarrubí et al., "Numerical evaluation of bimetallic self-adaptive fins acting as flow disturbing elements inside a microchannel," 2022 21st IEEE Intersociety Conference on Thermal and Thermomechanical Phenomena in Electronic Systems (iTherm), 2022, pp. 1-7, doi: 10.1109/iTherm54085.2022.9899648.
8. Angel, G. D., & Haritos, G. (2013). An immediate formula for the radius of curvature of a bimetallic strip. International Journal of Engineering Research &Technology, 2(12), 1312-1319
9. A. M. Khatkhate and A. Danpurwala,"Simulation Studies of a Novel Formula for Predicting the Radius of Curvature of a Bimetallic Strip," i-Manager's Journal on Material Science, vol. 8, p. 17, 2020
10. Khatkhate, A., Singh, R. & Mirchandani, P. T. (2017). An Elastic Moduli Independent Approximation to the Radius of Curvature of the Bimetallic strip. Material Science Research India, Vol. 14, 68–78.
11. K.N. Nikitin, V.Y. Osadchii, A.V. Saf, et al. Production of seamless bimetallic pipe for the nuclear industry Steel Transl, 47 (7) (2017), pp. 491-496

12. Li, Z.; Rezaei, S.; Wang, T.; Han, J.; Shu, X.; Pater, Z.; Huang, Q. Recent advances and trends in roll bonding process and bonding model: A review. Chin. J. Aeronaut. 2022.
13. Sas-Boca I-M, Iluțiu-Varvara D-A, Tintelecan M, Aciu C, Frunză DI, Popa F. Studies on Hot-Rolling Bonding of the Al-Cu Bimetallic Composite. Materials. 2022; 15(24):8807. https://doi.org/10.3390/ma15248807
14. Moisseytsev, Anton, and Filippone, Claudio. Load Following Analysis of the Holos-Quad 10MWe Micro-Reactor with Plant Dynamics Code. United States: N. p., 2022. Web. doi:10.2172/1877020.
15. Anton Moisseytsev, Claudio Filippone, Load Following Analysis of the Holos-Quad Micro Reactor, ANS Transactions / Volume 125 / Number 1 / December 2021 / Pages 1196-1199
16. Muhammad Talha Khan, Muhammad Javaid Afzal, F. Javaid, S. Tayyaba, Muhammad Waseem Ashraf, and Md. Khalid Hossain, "Study of tip deflection on a copper-steel bimetallic strip by fuzzy logic and ansys static structural," Proc. Int. Exch. Innov. Conf. Eng. Sci., 7 255–260 (2021). doi:10.5109/4738596.
17. Sedighi, M. and Dardashti, B.N. (2012). A review of thermal and mechanical analysis in single and bi-layer plate. Materials Physics and Mechanics, 14(1), 37–46.
18. C.E. Gillaume, Invar and its applications, Nature, 71 (1904), pp. 134-139
19. Aldalur E, Suárez A, Veiga F. Thermal expansion behaviour of Invar 36 alloy parts fabricated by wire-arc additive manufacturing. J Mater Res Technol 2022;19:3634–45. https://doi.org/10.1016/j.jmrt.2022.06.114.
20. SOLIDWORKS Simulation 2019 Validation report, https://www.solidworks.com/sites/default/files/2019-04/VPCS-English2019.pdf